



## Abstract

The isotopic composition of Si in biogenic silica (BSi), such as opal buried in the oceans' sediments, has changed over time. Paleo records suggest that the isotopic composition, described in terms of  $\delta^{30}\text{Si}$ , was generally much lower during glacial times than today. There is consensus that this variability is attributable to differing environmental conditions at the respective time of BSi production and sedimentation. The detailed links between environmental conditions and the isotopic composition of BSi in the sediments are, however, controversially discussed in the literature. In this study, we explore the effects of a suite of offset boundary conditions during the LGM on the isotopic composition of BSi archived in sediments in an Earth System Model of intermediate complexity. Our model results suggest that a change in the isotopic composition of Si supply to the glacial ocean is sufficient to explain the observed overall low(er) glacial  $\delta^{30}\text{Si}$  in BSi. All other processes explored triggered model responses of either wrong sign or magnitude, or are inconsistent with a recent estimate of bottom water oxygenation in the Atlantic Sector of the Southern Ocean. Caveats, mainly associated with generic uncertainties in today's pelagic biogeochemical modules, remain.

## 1 Introduction

Numerical, model-based projections into our warming future suggest ensuing global-scale redistribution of nutrients from the sun-lit surface ocean to depth. Among the prospective consequences are declining biological productivity and fish yields. Disconcertingly, these effects may prevail for a millennium (Moore et al., 2018). But how reliable are such climate projections?

The problem is that we will not live to calculate substantiated statistics on the reliability of climate forecasts. Hence, an approach similar to the one pursued in weather-forecasting, where progress has been accomplished during decades of daily forecasts and subsequent ground-truthing (c.f. Bauer et al., 2015), is not viable – if pressing societal questions are to be answered in time. A straight-forward and generic way to deal with this problem is to assume that fidelity of now-casts is correlated with the fidelity of climate forecasts. This assumption, however, has been challenged, e.g., by Knutti et al. (2009) and Notz (2015) for coupled ocean-atmosphere models and, recently, by Löptien and Dietze (2017) and Löptien and Dietze (2019) for models of pelagic biogeochemical cycling.

A potential solution to this dilemma is the assessment of past climate states to test the sensitivity of climate models (as suggested by, e.g., Braconnot et al., 2012). The idea being that the geologic records of environmental responses to past climate changes complement the climate observations from the past decades such that respective fidelity metrics become indicative of the reliability of future projections.

To this end, the isotopic composition ( $\delta^{30}\text{Si}$ ) of biogenic silica (BSi) preserved in ocean sediments is of special interest to the field of pelagic biogeochemical ocean modeling. The reasons are: first, silicic acid (DSi) is an essential element for diatoms, which are autotrophic key players in the pelagic carbon cycle. Second, the isotopic composition of BSi is stable and preserves over millennia, once secluded from processes at the water-sediment interface. Third, diatoms produce BSi with a  $\delta^{30}\text{Si}$  distinctly different from the  $\delta^{30}\text{Si}$  of their substrate DSi. The latter is caused by diatoms which tend to build more light BSi into their shells, compared to the  $\delta^{30}\text{Si}$  in ambient DSi - a process also referred to as fractionation. This fractionation relates the  $\delta^{30}\text{Si}$  of BSi in the sediments to the turnover of DSi by diatoms. The advantage of using the isotopic composition to improve our current understanding of glacial-interglacial cycles, instead of simply using BSi sediment burial rates, is that  $\delta^{30}\text{Si}$  is less affected by water-column processes which are, on the one hand, unrelated to BSi production but may, on the other hand, modulate the amount of BSi that is preserved in the sediments.

68 A major challenge is the interpretation of  $\delta^{30}\text{Si}$  of BSi records because the link be-  
69 tween diatom DSi turnover and  $\delta^{30}\text{Si}$  isotopic signature in BSi is complex (see also Rague-  
70 neu et al., 2000). In a (Rayleigh) system, like a surface mixed layer in spring, diatoms  
71 preferentially take up lighter DSi until only relatively heavy substrate is left (and sub-  
72 sequently taken up). Hence, the  $\delta^{30}\text{Si}$  isotopic signature in BSi is indicative of the amount  
73 of substrate left, with high (low) values indicating oligotrophic (nutrient replete) con-  
74 ditions. In contrast, in a system characterized by high incoming and outgoing physical  
75 transports of substrate (e.g. a location within the Gulf Stream) the  $\delta^{30}\text{Si}$  of BSi is pre-  
76 dominantly determined by the  $\delta^{30}\text{Si}$  of the constantly resupplied DSi - and only mod-  
77 estly altered by the respective fractionation during BSi production because the fraction-  
78 ation signal can not build up (since it is constantly flushed out of the local system). Both  
79 the Rayleigh and the "flushed" system can be described to high precision by simple equa-  
80 tions (e.g. Cloos et al., 2016, their equation 1 to 6). The difficulty is in the quantifi-  
81 cation of the relation between physical transport flushing rate and biotic BSi export out  
82 of the sun-lit surface ocean - or in other words: the relation between flushing and BSi  
83 production needs to be known in order to interpret  $\delta^{30}\text{Si}$  of BSi records.

84 In summary, both local (production and export of BSi, which is affected by local  
85 environmental conditions) and remote processes (production and export upstream which  
86 affects incoming environmental conditions), determine the isotopic signature of BSi at  
87 a given location. This complex entanglement of ocean circulation and biogeochemistry  
88 calls for the application of a 3-dimensional numerical model to guide the interpretation  
89 of  $\delta^{30}\text{Si}$  in observed BSi records. Indeed, the (modern climate) pioneering studies of Wis-  
90 chmeyer et al. (2003) and Gao et al. (2016) illustrated the benefit of using a numerical  
91 coupled ocean-circulation biogeochemical model in linking silicon isotopes to silicic acid  
92 utilization.

93 Using models for interpretation in such ways leads, however, to a causality dilemma.  
94 Coupled ocean-circulation biogeochemical models rely on a number of assumptions and  
95 (often poorly known) model parameters (such as growth/death of phytoplankton and  
96 sinking of organic matter to depth). Most of these assumptions and parameters are not  
97 well constrained in the sense that different choices may result in an equally-good fit to  
98 present day observations - but simultaneously very different projections (e.g. Löptien and  
99 Dietze (2017), Löptien and Dietze (2019)). Thus, paleo records such as the isotopic com-  
100 position of BSi preserved in ocean sediments, are of great interest to assess and reduce  
101 such uncertainties. At the same time, these model uncertainties complicate the interpre-  
102 tation of simulated past marine biogeochemical cycling in general (e.g., Hülse et al., 2017)  
103 and of the isotopic composition of BSi preserved in ocean sediments in particular. An  
104 aggravating circumstance is that the observational records are still so sparse (even for  
105 present day  $\delta^{30}\text{Si}$  DSi), such that Hendry and Brzezinski (2014) conclude that the data  
106 set is "... inadequate to evaluate mechanisms leading to even the first-order distribution  
107 of isotopes of Si in the global ocean".

108 Even so, a number of very interesting hypothesis, explaining aspects of spatial and  
109 temporal variance in  $\delta^{30}\text{Si}$  of BSi records, have been rooted on the available observational  
110 records. Among them is the Silicic Acid Leakage Hypothesis (SALH, e.g., Brzezinski et al.  
111 (2002), Matsumoto et al. (2002), Matsumoto et al. (2014)): Today's Southern Ocean (SO)  
112 retains or traps DSi at the expense of more northward latitudes by a combination of deep  
113 and efficient BSi export and meridional overturning. Driven by the strong southern west-  
114 erly wind belt, deep, nutrient replete waters are brought to the surface at the Antarc-  
115 tic Divergence. The northward branch of the Divergence (which potentially exports DSi  
116 from the SO) is efficiently stripped of DSi by phytoplankton. So, by the time the wa-  
117 ter reaches the Polar Front and the formation sites of Subantarctic Mode Waters (SAMW)  
118 and Antarctic Intermediate Waters (AAIW) which spread northwards, most of the DSi  
119 has been exported as BSi to depth into the southward-flowing Circumpolar Deep Wa-  
120 ter (CDW). The CDW surfaces south of the Polar Front and, hence, the respective DSi

121 is thereby retained in the SO. The SALH postulates that this DSi trapping in the SO  
 122 was alleviated during glacial times triggered by e.g. enhanced iron supply: the enhanced  
 123 iron supply and associated physiological changes may have reduced the Si demands of  
 124 diatoms, relative to the need of bioavailable nitrogen. Thus, left-over DSi might have leaked  
 125 into the SAMW and AAIW and thereby could have left the SO. In summary, the SALH  
 126 assumes that more DSi might have been available outside the SO during glacial times.  
 127 A straightforward (Rayleigh) conclusion is that the glacial  $\delta^{30}\text{Si}$  was lower (as observed)  
 128 because, according to the above considerations, DSi should have been less limiting re-  
 129 lative to nitrogen.

130 The SALH and its relation to relatively low glacial  $\delta^{30}\text{Si}$  has, however, been recently  
 131 challenged by Frings et al. (2016) who concluded, based on a very comprehensive review,  
 132 that consistent shifts among different ocean basins from low glacial  $\delta^{30}\text{Si}$  to higher in-  
 133 terglacial  $\delta^{30}\text{Si}$  (0.5–1‰) may rather have been caused by a respective change in the  
 134 isotopic composition of land-ocean fluxes of Si.

135 Our study adds to the ongoing discussion by exploring various hypotheses poten-  
 136 tially triggering lower glacial  $\delta^{30}\text{Si}$  in an Earth System Model of intermediate complex-  
 137 ity. Our modeling approach builds on the pioneering works of Wischmeyer et al. (2003)  
 138 and Gao et al. (2016) for modern climate and applies our extended model to both the  
 139 Last Glacial Maximum and modern climate. Specifically, we explore the effects of (1)  
 140 differences in the Si:N ratios, mimicking alleviated iron limitation during the LGM (Mat-  
 141 sumoto et al., 2014), (2) differing winds during the LGM (e.g., Kohlfeld et al., 2012; McGee  
 142 et al., 2010; Sime et al., 2013), (3) differing Si supply to the ocean during the LGM (Frings  
 143 et al., 2016) and (4) a differing isotopic composition of Si supplied to the ocean during  
 144 the LGM (Frings et al., 2016). The underlying aim is to illustrate the complex entan-  
 145 glement of ocean circulation and biogeochemistry, which finally determines the isotopic  
 146 composition of  $\delta^{30}\text{Si}$  of BSi preserved in sediments.

## 147 2 Materials and Methods

### 148 2.1 Observations

149 We use the World Ocean Atlas 2009 data to assess our preindustrial (*PI*) simula-  
 150 tion. More specifically, we compare against annual mean climatologies of temperature  
 151 (Locarnini et al., 2010), salinity (Antonov et al., 2010), phosphate (Garcia et al., 2010)  
 152 and silicate (Garcia et al., 2010).

153 Silicon isotopic data in seawater ( $\delta^{30}\text{Si}$  of DSi) are put together from data published  
 154 in Beucher et al. (2008,1); Cardinal et al. (2005); De La Rocha et al. (2011); de Souza  
 155 et al. (2012a,1); Ehlert et al. (2012); Fripiat et al. (2011a,1,1); Grasse et al. (2013); Reynolds  
 156 et al. (2006). A binning procedure increased horizontal data coverage: surface data with  
 157 a nominal depth of 50 m refers to binning all data within 0-100 m. Abyssal data with a  
 158 nominal depth refers to binning all data within 1500-2500 m.

159 Silicon isotopic data in BSi as preserved in sediment cores is compiled, following  
 160 Frings et al. (2016), from Brzezinski et al. (2002); De LaRocha et al. (1997); De La Rocha  
 161 et al. (1998, 2011); Ehlert et al. (2013); Ellwood et al. (2010); Hendry et al. (2012); Horn  
 162 et al. (2011); Pichevin et al. (2009).

### 163 2.2 Model

164 In this study we present numerical simulations with the University of Victoria Earth  
 165 System Climate Model (UVic ESCM, Weaver et al., 2001). We present equilibrium sim-  
 166 ulations for two distinct climates, the preindustrial year 1800 (PI) and the Last Glacial  
 167 Maximum (LGM) 21000 years before present and evaluate the model’s distribution of  
 168  $\delta^{30}\text{Si}$  of BSi preserved in ocean sediments. UVic ESCM is an intermediate complexity

169 model, featuring a simplified (vertically integrated) atmosphere. In contrast, the ocean  
 170 dynamics is, although rather coarse, resolved in all three dimensions. The vertical res-  
 171 olution starts with 50 m at the surface of the ocean and gradually coarsens to 500 m in  
 172 the abyss. The horizontal resolution of all model components (i.e., ocean, land, atmo-  
 173 sphere, sea ice) is 1.8° in meridional and 3.6° in zonal direction. UVic’s assets are low  
 174 computational demands and an extensive number of peer-reviewed studies including the  
 175 description of LGM and PI equilibrium simulations. Among its drawbacks are a simpli-  
 176 fied atmosphere and a spatial resolution of the ocean that is coarse compared to, e.g.,  
 177 that class of models that underlie the current projections of the Intergovernmental Panel  
 178 on Climate Change. Our simulations build on two configurations introduced by Bren-  
 179 nan et al. (2012) already:

180 (1) *PI*, which refers to the "Preindustrial Equilibrium Simulation" described in Sec.  
 181 3 of Brennan et al. (2012). Briefly summarized, the atmospheric  $p\text{CO}_2$  is set to 283.87 ppm  
 182 and the orbital configurations to those representative of the year 1800. The initial con-  
 183 ditions are those from the 5 kyr spinup from Brennan et al. (2012).

184 (2) *LGM*, which refers to the "Last Glacial Maximum Equilibrium Simulation" de-  
 185 scribed in Sec. 4 of Brennan et al. (2012). Briefly summarized, the atmospheric  $p\text{CO}_2$   
 186 is set to a low 189.65 ppm, the orbital parameters to those representing the conditions  
 187 at 21 kyr BP and the surface elevation and albedo on land are adjusted following a re-  
 188 construction of Northern Hemisphere land ice (ICE-4G, Peltie (2009))..

189 The wind forcing during LGM consists of the same prescribed climatology (NCEP)  
 190 used for the preindustrial simulations in our rather simple ESCM (see Weaver et al., 2001,  
 191 for details). Rather weak dynamic wind feedbacks are parameterized as a function of sur-  
 192 face temperature gradients and added to this climatology. The choice of building on a  
 193 present day climatology is pragmatic, since the wind conditions during the LGM are dis-  
 194 cussed controversially (e.g. Kohlfeld et al., 2012; Sime et al., 2013).

### 195 **2.2.1 Equations for the Si-Cycle**

196 For this study we added an explicit and prognostic representation of (1) dissolved  
 197 silicic acid (DSi), (2) biogenic Si (BSi), (3) that fraction of DSi that is composed of the  
 198 silicon isotope  $^{30}\text{Si}$  ( $\text{D}^{30}\text{Si}$ ) and (4) that fraction of BSI that is composed of the silicon  
 199 isotope  $^{30}\text{Si}$  ( $\text{B}^{30}\text{Si}$ ) to the original pelagic biogeochemical module used in Brennan et al.  
 200 (2012). All prognostic biogeochemical variables  $C$ , at a given point in (model) space are  
 201 determined following:

$$\frac{\partial C}{\partial t} = T + sms, \quad (1)$$

202 where  $T$  denotes the spatial divergence of diffusive and advective transports.  $sms$  refers  
 203 to the source-minus-sinks term. The  $sms$  terms of the silicon module are adopted from  
 204 Gao et al. (2016). The convenience of their approach is that the silicon module does not  
 205 feed back onto the original biogeochemical model (of, in our case, Brennan et al. (2012)).  
 206 Thus, our silicon isotope module is purely diagnostic in the sense that it does not alter  
 207 the original climate and carbon cycles documented by Brennan et al. (2012) already.

208 The respective  $sms$  terms that describe the linkage of the silicic acid cycle with the  
 209 pelagic biogeochemical cycle of Brennan et al. (2012) are described below. Approach and  
 210 notation follow Gao et al. (2016). The DSi is supplied to the ocean at a temporally con-  
 211 stant rate,  $RRDSi$  of  $9.55 \text{ Tmol Si year}^{-1}$  (Frings et al., 2016) and is homogeneously  
 212 distributed over the surface ocean.

213

• **DSi equation:**

$$sms(DSi) = r BSi - P_{Si}, \quad (2)$$

214

215

where  $r$  denotes the diatom opal dissolution rate and  $P_{Si}$  denotes the biogenic opal production.  $r$  is temperature dependent:

$$r = A \exp(T/T_c), \quad (3)$$

216

217

218

219

220

221

with the parameters  $A$  setting the dissolution rate and  $T_c$  determining the temperature dependence of opal dissolution. The value of  $T_c$  is adopted from Gao et al. (2016) (see Table 1). The value of  $A$  has been determined in a tuning exercise (see Section 2.2.2),  $P_{Si}$  is calculated as a function of the production rate of particulate organic matter  $pomp$  (as calculated by the original biogeochemical module of Brennan et al., 2012) and DSi concentration:

$$P_{Si} = \min \left( pomp R_{Si:P} \frac{DSi}{K_{PHY}^{DSi} + DSi}, r_{Pro} DSi \right), \quad (4)$$

222

223

224

225

where,  $R_{Si:P}$  denotes the molecular DSi to phosphate uptake ratio, associated with BSi production,  $K_{PHY}^{DSi}$  denotes the half-saturation constant of DSi uptake (see Table 1).  $r_{Pro}$  is the maximum rate of BSi production under non-limiting conditions.

226

• **BSi equation:**

$$sms(BSi) = -r BSi + P_{Si} - w \frac{\partial BSi}{\partial z}, \quad (5)$$

227

228

where,  $w$  is the sinking speed of BSi and  $w \frac{\partial BSi}{\partial z}$  denotes the divergence of vertical BSi fluxes.

229

• **D<sup>30</sup>Si equation:**

230

231

232

233

234

Following Gao et al. (2016) we include, in addition to total Si (i.e. the sum of the stable isotopes <sup>28</sup>Si, <sup>29</sup>Si, and <sup>30</sup>Si), an explicit representation of the silicon isotope <sup>30</sup>Si. During BSi production we apply the fractionation factor  $\alpha_1 = 0.9989$  (De LaRocha et al., 1997; Gao et al., 2016) which reduces the uptake of heavier <sup>30</sup>Si relative to the lighter Si stable isotopes.

$$sms(D^{30}Si) = r BSi \frac{B^{30}Si}{BSi} - P_{Si} \alpha_1 \frac{D^{30}Si}{DSi} \quad (6)$$

235

Following Gao et al. (2016), we assume no fractionation during BSi dissolution.

236

• **B<sup>30</sup>Si equation:**

$$sms(B^{30}Si) = -r BSi \frac{B^{30}Si}{BSi} + P_{Si} \alpha_1 \frac{D^{30}Si}{DSi} - w \frac{\partial B^{30}Si}{\partial z}. \quad (7)$$

237

238

We calculate the silicon isotopic composition  $\delta^{30}Si$  in units ‰ as a function of the total DSi (or BSi) concentration and D<sup>30</sup>Si (or B<sup>30</sup>Si) following:

$$\delta^{30}Si = \left( \frac{({}^{30}Si/{}^{28}Si)_{sample}}{({}^{30}Si/{}^{28}Si)_{NBS-28}} - 1 \right) \cdot 10^3, \quad (8)$$

239

240

241

242

243

244

245

246

$({}^{30}Si/{}^{28}Si)_{NBS-28} = 0.0335$  (Coplen et al., 2002). We calculate  ${}^{28}Si$  from the total Si and <sup>30</sup>Si concentrations as  ${}^{28}Si = 0.953(Si - {}^{30}Si)$  which assumes that all stable isotopes other than the <sup>28</sup>Si and <sup>30</sup>Si always amount to 4.7% of total Si. (Here we follow Reynolds, 2009, stating that the assumption of a constant relative abundance of the normalizing isotope "... is valid for small isotopic variations described by the  $\delta$  notation".)

We set the isotopic composition  $\delta^{30}Si$  of DSi supplied to the surface ocean (mimicking e.g. river runoff)  $RR\delta^{30}$  to 0.74 (Frings et al., 2016).

**Table 1.** Reference model parameters of our implementation of the Gao et al. (2016) silicon module into the pelagic biogeochemical module of Brennan et al. (2012).

parameter	description	Gao et al. (2016)	our value	unit
$A$	opal dissolution rate	$333^{-1}$	$90^{-1}$ (see Fig. 1)	$\text{day}^{-1}$
$T_c$	critical temperature of opal dissolution	12	12	$^{\circ}\text{C}$
$R_{Si:P}$	molecular DSi to phosphate stoichiometric ratio	25	25	$\frac{\text{mol DSi}}{\text{mol P}}$
$K_{PHY}^{DSi}$	half-saturation constant of DSi uptake during BSi production	4	4	$\frac{\text{mmol DSi}}{\text{m}^3}$
$r_{Pro}$	BSi production rate under non-limiting conditions	0.5	0.5	$\text{day}^{-1}$
$w$	sinking speed of BSi	10	10	$\frac{\text{m}}{\text{day}}$
RRDSi	total Si supply to the (surface) ocean (by e.g. river runoff)	9	9.55 (Frings et al., 2016)	$\frac{\text{Tmol Si}}{\text{year}}$
$\text{RR}\delta^{30}$	isotopic composition of (riverine) Si supply to the (surface) ocean	0.8	0.74 (Frings et al., 2016)	$\text{‰}$
$\alpha_1$	$^{30}\text{Si}$ fractionation factor during BSi production	0.9989	0.9989	$\square$
$\square$	fractionation factor during BSi dissolution	1	1	$\square$

247 Our implementation of processes in the sediments is idealized. Once BSi sinks out of the  
 248 lowermost wet model grid box it gets buried and leaves the system forever. A constant  
 249 surface flux RRDSi (Table 1) replenishes what is lost by sedimentation - if the integra-  
 250 tion is long enough so that the model can reach an equilibrium. Simulated  $\delta^{30}\text{Si}$  of sed-  
 251 imented BSi are taken as the simulated isotopic composition of BSi sinking out of the  
 252 lowermost wet model grid box. This idealization is motivated by the urge to save com-  
 253 putational resources that would otherwise be necessitated to equilibrate the sediment  
 254 model.

### 255 2.2.2 Parameter Settings

256 The volume of the ocean is  $1.4 \cdot 10^{18} \text{ m}^3$ , containing an average DSi concentration  
 257 of  $92 \text{ mmol Si m}^{-3}$  (Garcia et al., 2010). This yields an oceanic inventory of  $1.3 \cdot 10^{17} \text{ mol Si}$ .  
 258 Devision of the inventory with the supply rate of DSi (RRDSi, Table 1) to the ocean yields  
 259 a timescale of 14 000 years (which is slightly less than the 16 000 years estimated by Tréguer  
 260 et al., 1995). This timescale is a rough estimate of the residence time of DSi in the ocean.

261  
262

As such it provides a lower bound on the time our model framework needs to adjust to changes to the formulation of Si cycling. It is also a measure of the expected equilibration timescale of the model.

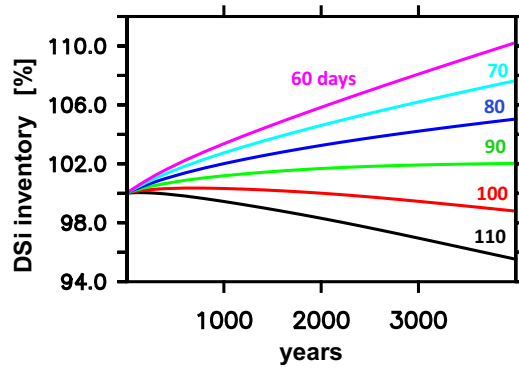


**Figure 1.** Temporal evolution of simulated preindustrial oceanic DSi inventory relative to observations (WOA09 Garcia et al., 2010, also used to initiate the model) in units %. The different colors denote simulations with different opal dissolution rates (i.e. different choices of parameter  $A$  in Table 1). The colored numbers denote the respective inverse of parameter  $A$  in units days.

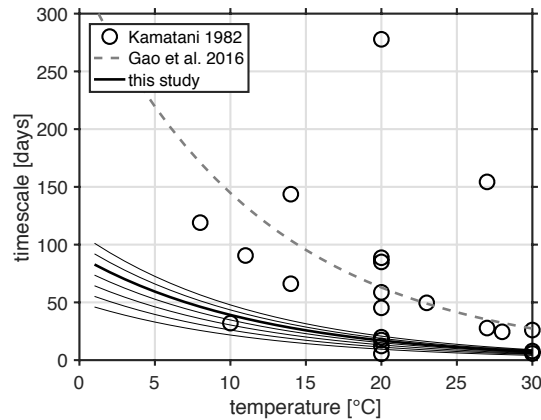


**Figure 2.** Inverse of dissolution rates of silica from diatoms as a function of ambient temperature. The circles denote data compiled by Kamatani (1982). Three values in excess of 300 days have been discarded here. The dashed grey line refers to settings in the model of Gao et al. (2016). The thick black line refers to the reference model setting in this study. The thin black lines refer to settings tested during tuning the DSi inventory.

263

264  
265  
266  
267  
268  
269  
270

The long equilibration timescale of our Si module calls for long wall-clock times until the effects of model changes can be evaluated reliably. This limits the number of model parameters (and formulations) that can be explored. Our approach here is to use the original model formulations and parameters from Gao et al. (2016) and to adjust only the opal dissolution rate  $A$ , such that the DSi inventory stays close to the observations from Garcia et al. (2010). Fig. 1 shows that, to this end, the choice of  $A = 90^{-1} \text{ days}^{-1}$  is the best compromise between fast equilibration (which saved wall-clock time) and small

271 misfit to observations (only two % overestimation of DSi inventory) among the choices  
 272 of  $A$  tested in this study.

273 Fig. 2 shows the temperature dependance of silica dissolution rates that is asso-  
 274 ciated with our choice of  $A$ : compared with Gao et al. (2016), our choice features sub-  
 275 stantially faster dissolution rates, throughout the entire range of temperatures. When  
 276 compared to data compiled by Kamatani (1982) it is, however, still consistent with ob-  
 277 servations. On these grounds we justify our choice of  $A = 90^{-1}$ . We provide a respec-  
 278 tive model assessment for the Si module in the Appendix A.

### 279 **2.2.3 Experiments**

280 As outlined above (Sect. 2.2), we run our reference model version under PI and LGM  
 281 climate conditions to quasi-equilibrium (simulations *PI* and *LGM*). In a second step, start-  
 282 ing from *LGM*, we perform a suite of sensitivity experiments for the LGM. Table 2 lists  
 283 these experiments, tailored to explore the sensitivity of our model towards environmen-  
 284 tal changes. The focus is on changes that have been suggested in the literature to have  
 285 engrained substantial signatures in the isotopic composition of  $\delta^{30}\text{Si}$  of the BSi archived  
 286 in oceanic sediments. These simulations are setup as follows:

- 287 • *LGMfe* is designed to mimic the effect of iron replete conditions on DSi uptake.  
 288 As summarized by Matsumoto et al. (2014), there is evidence from incubation ex-  
 289 periments that the Si:N consumption ratio is high under iron-depleted conditions  
 290 (Franck et al., 2000; Hutchins and Bruland, 1998) and relatively low under iron  
 291 replete conditions (Franck et al., 2000; Pondaven et al., 2000). In experiment *LGMfe*  
 292 the molecular DSi to phosphate stoichiometric ratio  $R_{\text{Si:P}}$  is reduced by 36%. Be-  
 293 cause the N:P ratio is fixed to 16 in our model, this corresponds to a Si:N ratio  
 294 of 1.
- 295 • *LGMbreezy* and *LGMslack* are designed to test the effect of potential glacial in-  
 296 terglacial variability of climatological winds driving the ocean circulation: The wind  
 297 conditions during the LGM are discussed controversially, such that even the sign  
 298 of changes relative to today's conditions is uncertain (e.g. Kohlfeld et al., 2012;  
 299 McGee et al., 2010; Sime et al., 2013). In order to envelope the range of poten-  
 300 tial effects on  $\delta^{30}\text{Si}$  of BSi, we follow Matsumoto et al. (2014) and test both a global  
 301 doubling of wind speeds and a bisection, dubbed *LGMbreezy* and *LGMslack*, re-  
 302 spectively. These changes affect only the momentum received by the ocean.
- 303 • *LGMflush* and *LGMtrickle* are designed to test the effect of potential glacial in-  
 304 terglacial variability of riverine Si inputs into the ocean. Following Frings et al.  
 305 (2016), who suggest, based on a literature review, that the river DSi flux has been  
 306 within  $\pm 20\%$  of today's inputs during the LGM, we increase (decrease) the total  
 307 supply of Si to the surface ocean by 20% in experiment *LGMflush* (*LGMtrickle*).  
 308 Because reliable data regarding the variability of the spatial distribution of this  
 309 input over time is sparse we distribute all input evenly over space.
- 310 • *LGMlight* is designed to test the idea of Frings et al. (2016) that the relatively low  
 311 values of  $\delta^{30}\text{Si}$  archived in glacial BSi are caused by an isotopically lighter com-  
 312 position of riverine Si inputs to the ocean. Following Frings et al. (2016), *LGM-*  
 313 *light* reduces the  $\delta^{30}\text{Si}$  of DSi supplied to the ocean by 1‰. The underlying idea  
 314 is that biotic and abiotic processes acting along the course of a river determine  
 315 the isotopic composition of the runoff to the ocean. To this end, the study of Schoe-  
 316 lynck et al. (2019) is a very illustrative curiosity showing the effect of a herd of  
 317 hippos increasing  $\delta^{30}\text{Si}$  by a sizable 0.2‰ in Mara River, Kenya.

**Table 2.** Model simulations.

tag	description	initial conditions	duration of simulation
<i>PI</i>	"Preindustrial Equilibrium Simulation" of Brennan et al. (2012)	equilibrated simulation of Brennan et al. (2012)	10000 yr
<i>LGM</i>	"Last Glacial Maximum Equilibrium Simulation" of Brennan et al. (2012)	equilibrated simulation of Brennan et al. (2012)	20000 yr
<i>LGMfe</i>	identical to <i>LGM</i> except for Si:N stoichiometric ratio reduced to 1, mimicking the effect of iron replete conditions	end of LGM	10000 yr
<i>LGMbreezy</i>	identical to <i>LGM</i> except for a doubling in all winds, driving the oceanic circulation	end of LGM	10000 yr
<i>LGMslack</i>	identical to <i>LGM</i> except for a bisection of all winds, driving the oceanic circulation	end of LGM	10000 yr
<i>LGMflush</i>	identical to <i>LGM</i> except for 20% increase in land-ocean DSi supply	end of LGM	10000 yr
<i>LGMtrickle</i>	identical to <i>LGM</i> except for 20% decrease in land-ocean DSi supply	end of LGM	10000 yr
<i>LGMlight</i>	identical to <i>LGM</i> except for a 1‰ decrease in $\delta^{30}\text{Si}$ of land-ocean DSi supply	end of LGM	10000 yr

### 2.3 Manifestation Timescales

Our model investigations are all based on numerical time-slice experiments (i.e., we run the model to quasi-equilibrium under the respective boundary conditions) - as opposed to investigating transient responses. Such an approach discards the information regarding the timescales on which model responses to disturbances manifest themselves. This can spuriously illuminate links between processes and their manifestation in the isotopic composition of material archived in sediment cores. We thus measure "manifestation timescales" by locally fitting exponential functions to the simulated  $\delta^{30}\text{Si}$ -anomalies in BSi of the 10 000 year sensitivity experiments, listed in Table 2. Depending on the sign of changes in  $\delta^{30}\text{Si}$  in BSi we fit either to:

$$f(t, x, y) = \alpha(x, y)e^{-\frac{t}{\tau(x, y)}}, \quad (9)$$

or

$$f(t, x, y) = \alpha(x, y) \left(1 - e^{-\frac{t}{\tau(x, y)}}\right), \quad (10)$$

where  $f(t, x, y)$  is the accumulated change in  $\delta^{30}\text{Si}$  of BSi at time  $t$ , longitude  $x$  and latitude  $y$ . The constant  $\alpha(x, y)$  and the manifestation timescale  $\tau(x, y)$  are estimated by using an unconstrained nonlinear minimization of the root mean square deviation between the local exponential fit and simulated local changes in  $\delta^{30}\text{Si}$  in BSi (Nelder–Mead, described in e.g. Lagarias et al., 1998, starting with an initial guess of  $\tau = 100 \text{ years}$  and  $\alpha(x, y)$  as the difference of  $\delta^{30}\text{Si}$ -anomalies between the start and the end of respective time slice experiments).

## 3 Results

In the following subsections we explore the results of the sensitivity experiments regarding their ability to reproduce observed differences in the  $\delta^{30}\text{Si}$  signature between LGM and PI. Each of the sensitivity experiments builds on a scenario of environmental LGM conditions proposed earlier in the literature (see Section 2.2.3; Table 2). The major aim is to dissect mechanisms that lead to reasonable agreement with the observations and paleoarchive data.

### 3.1 LGM

Figure 3 panel (a) shows the difference between the LGM "reference" simulation *LGM* and our preindustrial simulation *PI*. We find that the colder glacial climate, overall, increases  $\delta^{30}\text{Si}$  of BSi deposited to the sediments (relative to PI). This is inconsistent with observations typically featuring lower glacial  $\delta^{30}\text{Si}$ . (An exception to this rule is the Atlantic Ocean where simulated glacial  $\delta^{30}\text{Si}$  of BSi are lower and roughly consistent with observations.)

In order to set a reference point for the following discussions (in this Section) we dissect the processes that imprint the wrong sensitivity into simulation *LGM*: key to understanding is that *LGM* features an oceanic DSi inventory that is 15% lower relative to that in *PI*. This is puzzling because the export of BSi across 120 m depth (which constitutes the origin of all BSi sinking to depth) is also reduced by a substantial 30% during the colder LGM climate. Given that the riverine supply of Si is identical in *LGM* and *PI*, this is counterintuitive. Further investigations revealed that the process behind this conundrum is the antagonistic effect of temperature on BSi sedimentation rate in our model framework. *LGM* features, consistent with observational evidence (e.g., Margo Project Members, 2009), an average of 2°C colder oceanic temperature than *PI*. In combination with an increase in sea-ice cover during the LGM, which shields the ocean from photosynthetically active radiation essential for autotrophic growth, this slows down the global primary production and associated export of organic material from the sun-lit surface

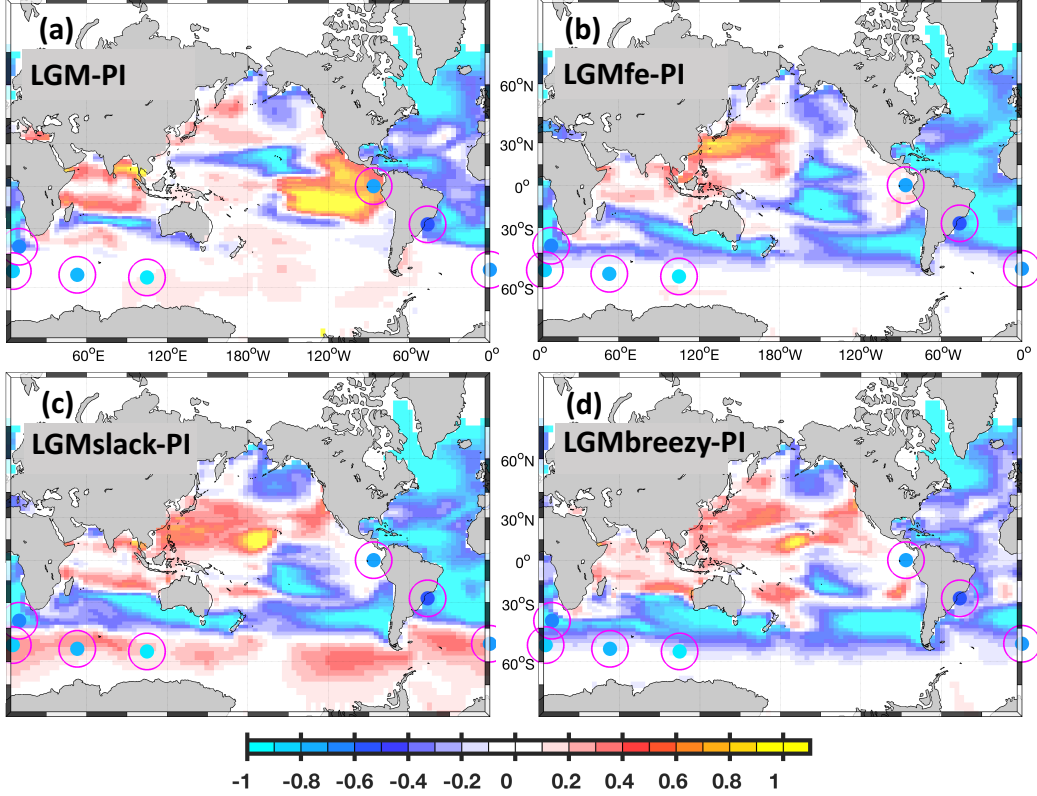


**Figure 3.** Difference in simulated  $\delta^{30}\text{Si}$  of BSi relative to the preindustrial simulation  $PI$  as deposited to sediments in units ‰. Panel (a), (b), (c) and (d) refer to differences  $LGM-PI$ ,  $LGMfe-PI$ ,  $LGMslack-PI$  and  $LGMbreezy-PI$ , respectively. Magenta circles denote locations of observations of  $\delta^{30}\text{Si}$  in BSi as preserved in sediment cores (see Section 2.1).

363 to depth. Hence, less BSi is produced and less BSi is set on its way sinking to the sed-  
 364 iments. This reduction in BSi production is, however, overcompensated by a reminer-  
 365 alization rate that is also slowed down by the lower temperatures such that more organic  
 366 material reaches the seafloor before it is remineralized and dissolved. A rough scaling,  
 367 assuming steady state (and horizontal uniformity which reduces the problem to one spa-  
 368 tial dimension), puts the potential of this effect into perspective: the vertical flux of sink-  
 369 ing BSi described in Equation 5 is, following the notation of Kriest and Oschlies (2008),  
 370 given by

$$F(z') = F_0 \exp\left(-\frac{rz'}{\bar{w}}\right), \quad (11)$$

371 where  $F(z')$  is the sinking flux at depth  $z'$  defined as that distance between actual depth  
 372 and the depth of the euphotic zone.  $F_0$  is the flux out of the euphotic zone. The sink-  
 373 ing speed  $\bar{w}$  is  $10 \text{ m day}^{-1}$  (see Table 1), and  $r$  as defined by our Equation 3. For an ocean  
 374 with a uniform temperature of  $4^\circ\text{C}$  Equation 11 (such as in  $PI$ ) yields a sedimentation  
 375 efficiency (here defined as the ratio between flux to the sediment and export out of the  
 376 euphotic zone) of 2‰. A reduction of temperature down to  $2^\circ\text{C}$  (such as in  $LGM$ ) yields  
 377 5‰. Hence, a reduction of only  $2^\circ\text{C}$  yields a substantial (initial) 2.5-fold increase in re-  
 378 spective sedimentation rates. It is this temperature-driven increase in sedimentation ef-  
 379 ficiency that reduces the global availability of DSi and, consequently, increases overall  
 380  $\delta^{30}\text{Si}$  in our  $LGM$  simulation relative to  $PI$ .

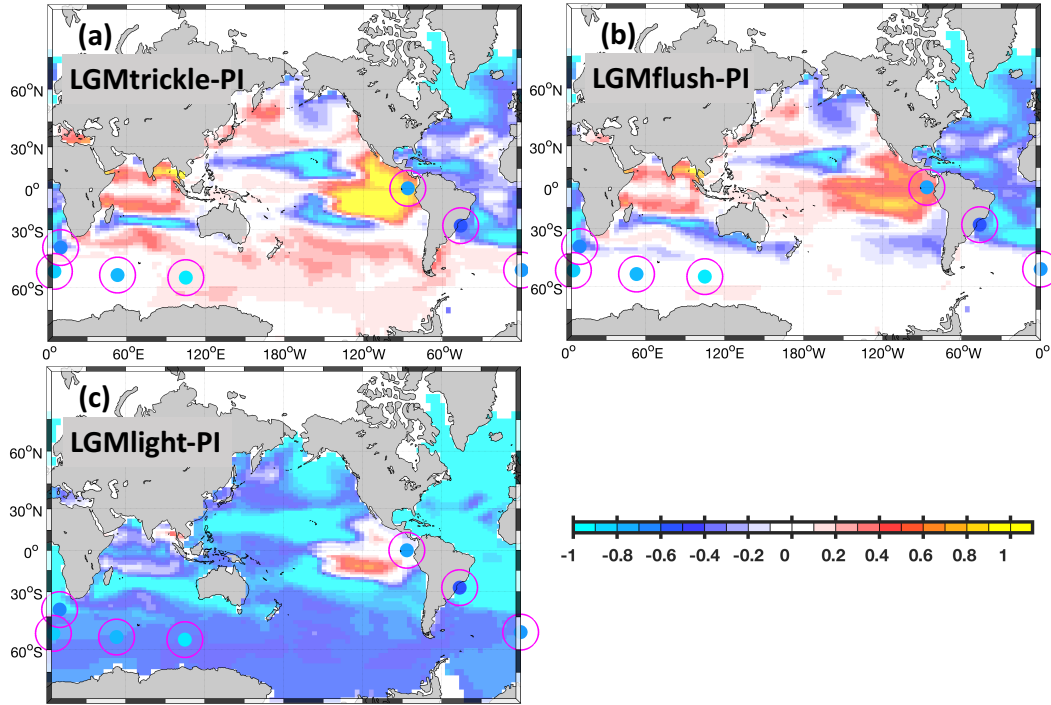


**Figure 4.** Difference in simulated  $\delta^{30}\text{Si}$  of BSi relative to the preindustrial simulation *PI* as deposited to sediments in units ‰. Panel (a), (b) and (c) refer to differences *LGMtrickle-PI*, *LGMflush-PI* and *LGMlight*, respectively. Magenta circles denote locations of observations of  $\delta^{30}\text{Si}$  in BSi as preserved in sediment cores (see Section 2.1).

381 As concerns the decreasing  $\delta^{30}\text{Si}$  of BSi in the Atlantic Ocean, which outweighs the  
 382 globally-reversed trend, we find: north of 55° N the simulated DSi inventory is substan-  
 383 tially higher during the LGM, relative to *PI* (Figure A.3). This is owed to fundamen-  
 384 tally different global circulation patterns in *PI* and *LGM*. In *PI* the upper branch of the  
 385 meridional overturning circulation (MOC) supplies the North Atlantic with surface wa-  
 386 ters that are already relatively depleted in DSi because of biologically induced BSi ex-  
 387 port from the surface to depth. The lower branch of the MOC exports deep waters en-  
 388 riched in BSi such that the DSi content of the Atlantic Ocean is relatively low. Simu-  
 389 lation *LGM* differs in that sea ice protrudes down to 52°N (in winter) which shields re-  
 390 spective algae from essential photosynthetically active radiation. This reduced verti-  
 391 cal export of BSi meets throttled meridional overturning circulation (2 Sv versus 18 Sv in  
 392 the simulation *PI*) which puts an end to the cycle that reduces the DSi inventory of the  
 393 Atlantic Ocean. The supply of DSi to the surface ocean is identical in *PI* and *LGM*. It  
 394 has a prescribed, relatively (compared to surface values in the North Atlantic) low  $\delta^{30}\text{Si}$   
 395 value of 0.74‰ and is evenly distributed over the ocean in our model (see Section 2.2.1).  
 396 This eventually reduces the  $\delta^{30}\text{Si}$  of BSi in the glacial Atlantic Ocean because it is no  
 397 longer (or far less) counteracted by the peculiar interplay between biology and MOC de-  
 398 scribed above.

### 399 3.2 LGMfe

400 The simulation *LGMfe* anticipates that more bioavailable iron was available dur-  
 401 ing the LGM. We mimic this effect by reducing the DSi demands by 36% relative to the  
 402 nitrogen (and phosphorous) demands in our model. This decelerates the biogeochem-

ical cycling of DSi which - according to the Silicic Acid Leakage Hypothesis (SALH) - would reduce the DSi trapping efficiency of the SO. The basic idea behind today's relatively efficient DSi trapping in the SO is that surface waters on their way north out of the SO get depleted of nutrients (DSi) by biologic (BSi) export to depth into southward moving water masses, thereby "trapping" DSi in the SO. By decelerating the cycling of DSi (e.g. by reducing the Si quota in sinking organic matter), the major trapping mechanism is weakened and the hypothesis is that this results in net DSi export, or leakage, out of the SO.

We define a measure of leakage or respective reduction in the "DSi trapping efficiency" as the ratio between oceanic inventory south of 40°S and the total global DSi inventory. Comparing *LGMfe* with *LGM* we find a reduction of only one percent. This rather minute change is outweighed by the effect of the the 36% reduction in DSi demands, described above, which leads to a substantially damped biogeochemical DSi cycling and a reduction of BSi export to the sediments. The latter results in a global increase in the oceanic DSi content of 11%. Hence, even though the trapping efficiency in the SO is reduced, the SO does not lose DSi but rather gains  $\approx 10\%$  relative to simulation *LGM*. The increase in both local (in the SO) and global DSi concentrations triggers an overall decrease in  $\delta^{30}\text{Si}$  of BSi (Fig. 3 panel (b)) which is generally roughly consistent with observations as far as the sign of changes in concerned. An exception being the SO, where simulated changes are too weak, and at some locations even of opposite sign when compared to the observations.

### 3.3 LGMslack and LGMbreezy

The simulations *LGMslack* and *LGMbreezy* assume, in contrast to the reference simulation, that glacial winds differed from those today. Sign and magnitude of the change is controversially discussed in the literature. Here we test both, a global bisection *LGMslack* and a doubling *LGMbreezy* of wind speeds. The results are depicted in Fig. 3, panels (c) and (d), with *LGMslack* featuring a generally higher  $\delta^{30}\text{Si}$  of BSi in the SO, suggesting a straightforward underlying process: reduced winds bring less DSi up to the sunlit surface which increases the effect of fractionating DSi uptake by algae in surface DSi (because there is less "flushing" of the system). As the substrate (surface DSi) becomes higher in  $\delta^{30}\text{Si}$ , so does the associated BSi export.

In contrast, in *LGMbreezy* more DSi is upwelled in the SO. The effect of fractionation on the isotopic composition of the substrate is diluted by the additional DSi supply. As a consequence  $\delta^{30}\text{Si}$  of BSi mostly decreases and is consistent with observations in terms of the sign of simulated changes. But specifically in the SO *LGMbreezy* features, a sensitivity which is apparently too low.

Complexity is added to the rest of the ocean as the system adjusts: enhanced (decreased) upwelling of nutrients by winds feed an increase (decrease) in export production which results in a global Si loss (gain) by increased (decreased) sedimentation such that the initial nutrient pulse is counteracted. Negative values, both in *LGMslack* and *LGMbreezy* follow the overall patterns already discussed for *LGM*.

In summary, our model suggests that reduced winds are inconsistent with observed  $\delta^{30}\text{Si}$  of BSi in the SO. In contrast, the effect of increasing winds appear to be more consistent with the observations of  $\delta^{30}\text{Si}$  of BSi as far as the sign of changes is considered. In terms of magnitude, however, a doubling of the wind during the LGM fails to retrace most of the observations in the SO.

### 3.4 LGMtrickle and LGMflush

The experiments *LGMtrickle* and *LGMflush* assume that the supply of Si to the glacial ocean was different from today's. The default value (applied in all of our config-

452 urations except the two discussed here) for total supply of Si to the ocean (RRDSi) is  
 453  $9.55 \text{ Tmol Si year}^{-1}$  with an isotopic composition corresponding to 0.74‰ (RR $\delta^{30}\text{Si}$ ; Ta-  
 454 ble 1). The fractionating effect of marine biota increases the global mean  $\delta^{30}\text{Si}$  of DSi  
 455 relative to the supply because it preferentially exports BSi with lower  $\delta^{30}\text{Si}$  to the sed-  
 456 iment such that DSi with higher  $\delta^{30}\text{Si}$  remains in the water column. From this we con-  
 457 clude that the larger (smaller) the supply in relation to the biotic turnover the lower (higher)  
 458 the  $\delta^{30}\text{Si}$  in DSi - which ultimately controls the isotopic composition of BSi archived in  
 459 sediments.

460 Fig. 4 supports this conclusion: panel (a) shows the difference between the simu-  
 461 lation *LGMrickle* and *PI*. Compared to panel (a) in Fig. 3, we find that the 20% reduc-  
 462 tion of Si supply to the ocean drives an overall increase in  $\delta^{30}\text{Si}$  of BSi. Likewise, panel  
 463 (b) in Fig. 4 shows that a 20% increase in Si supply decreases the overall  $\delta^{30}\text{Si}$  of BSi  
 464 with the biggest effect concentrated in the eastern equatorial upwelling area.

465 In summary, the sensitivity of  $\delta^{30}\text{Si}$  of BSi to changes in Si supply is too small to  
 466 explain observed glacial interglacial variations. Expressed in terms of a global average  
 467 of  $\delta^{30}\text{Si}$  of BSi, we find less than 0.1‰ change when altering the Si supply by 40% in Si.

### 468 3.5 LGMlight

469 Frings et al. (2016) suggest that the relatively low  $\delta^{30}\text{Si}$  of BSi archived in glacial  
 470 sediments are caused by a glacial isotopic composition of the Si supplied to the ocean  
 471 that was 1‰ lighter than today. Consistent with their reasoning, we find in Fig. 4 panel  
 472 (c) a global decrease in  $\delta^{30}\text{Si}$  of BSi by up to 1‰ (with the eastern tropical Pacific be-  
 473 ing an exception) in response to the reduction of RR $\delta^{30}\text{Si}$ . Expressed in terms of a global  
 474 oceanic average we find a decrease of 0.65‰ at the end of our 10 000 year spinup.

475 In summary, Fig. 4 panel (c) suggests that a reduction of  $\delta^{30}\text{Si}$  in DSi supplied to  
 476 the ocean drives changes that are consistent with almost all observations of glacial  $\delta^{30}\text{Si}$   
 477 in BSi archived in sediments.

## 478 4 Discussion

479 In Section 4.1 we discuss timescales at work, Section 4.2 puts the results into per-  
 480 spective and Section 4.3 discusses potential and generic sources of uncertainties in the  
 481 underlying Earth System Model.

### 482 4.1 Manifestation Timescales

483 So far we explored the sensitivity of our model to changes in environmental con-  
 484 ditions with numerical time-slice experiments. This can be deceptive for, e.g., processes  
 485 that manifest themselves with timescales as long or longer than typical glacial interglacial  
 486 cycles. In the following we use the concept of manifestation timescale introduced in Sec-  
 487 tion 2.3. in order to check if our simulated isotopic signatures of processes could possi-  
 488 bly be detected in actual sediments - as opposed to being smeared out over one or more  
 489 glacial interglacial cycles.

490 Fig. 5 shows that manifestation timescales vary considerably over space. In terms  
 491 of detectability, we find in *LGMrickle* that manifestation timescales at the observational  
 492 sites are short enough so that they should be detectable in sediments (if they were to  
 493 have been at play). This suggests that the effect of changing isotopic composition of oceanic  
 494 Si supply to the ocean would be clearly imprinted into the sediment record. This does  
 495 not apply to *LGMrisky* where manifestation timescales in the Southern Ocean exceed  
 496 5000 years (not shown).

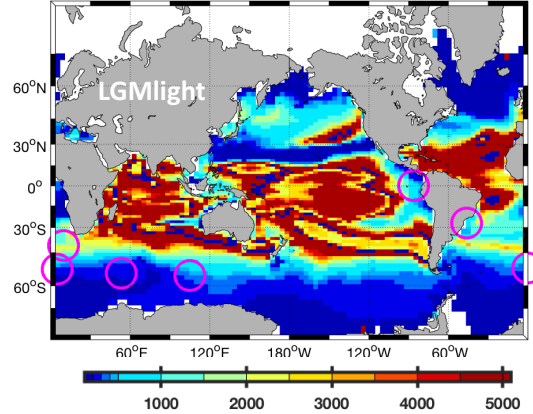


**Figure 5.** Timescale of manifestation of changes in  $\delta^{30}\text{Si}$  of BSi archived in sediments simulated in *LG Mlight* (as shown in Figure 3 panel c) in units years. White patches denote changes of less than 0.1‰ or regions with bottom BSi concentrations less than  $10^{-10} \text{ mol Si m}^{-3}$ . Magenta circles denote locations of observations of  $\delta^{30}\text{Si}$  in BSi as preserved in sediment cores (see Section 2.1).

497

## 4.2 Appraisal of Results

498

499

500

501

502

503

504

505

506

507

508

The two experiments *LG Mbreazy* and *LG Mlight*, out of our total of 7 numerical sensitivity experiments, feature the best fit with respect to the sign to the overall, lower (relative to today) glacial  $\delta^{30}\text{Si}$  of BSi observations. This holds especially in the Southern Ocean. The experiment with increased winds (*LG Mbreazy*), however, features a sensitivity which, although of correct sign, is much lower than suggested by observational evidence. In addition *LG Mbreazy* features very long manifestation timescales (when compared to *LG Mlight*; cf., Sect. 4.1) which implies that the process of increasing winds is, in reality, even harder to detect than the rather weak signal we find at the end of our 10 000 year long numerical time slice experiment suggests. This leaves us with simulation *LG Mlight* being the most consistent with observations of  $\delta^{30}\text{Si}$  of BSi out of all considered processes (listed, e.g., in Table 2).

509

510

511

512

513

514

515

516

517

518

519

520

521

522

523

524

525

526

527

Even so, other processes such as changes to air-sea iron fluxes and wind fields may also have been at play. According to our model results, however, these should manifest themselves more prominently in metrics other than in the isotopic composition of BSi. One example of such a metric are sedimentary redox-sensitive trace-metal records. Jaccard et al. (2016) deduce from respective evidence glacially reduced dissolved oxygen concentrations in the Atlantic Sector of the deep SO. Figure 6 suggests that, in our model, a decrease in wind speeds does drive a consistent oxygen decrease while unchanged winds, or an increase of winds, result in an inconsistent increase of simulated dissolved oxygen concentrations. Investigations of the link between decreasing winds and oxygen reveals two antagonistic processes being at work in our model. For one, the reduced wind-induced upwelling of nutrients drives less production and associated oxygen consumption in the SO. This, on its own, would increase the oxygen concentration. However, this process is opposed by a reduced wind-induced overturning which reduces ventilation and drives an oxygen decrease. The net effect differs among the sectors of the SO, such that the Atlantic Sector in Figure 6 panel (b) is consistent with results from Jaccard et al. (2016). The difference among the Sectors in the SO is facilitated by a reduced (down to 40% relative to *LGM*) Antarctic Circumpolar Current which reduces the zonal mixing between the Sectors as a result of reduced winds supplying less momentum to the ocean. Please note that a comprehensive analysis of oceanic deoxygenation, which must cover the role

528 of (preferably explicitly resolved) iron dynamics (see, e.g. Stoll, 2020) and more data (e.g.  
 529 Jaccard and Galbraith, 2011), is beyond the scope of this manuscript which focuses on  
 530 the isotopic composition of BSi in response to changing environmental conditions. Our  
 531 main conclusion here is that *LGMbreezy* is apparently inconsistent with sedimentary redox-  
 sensitive trace-metal records.

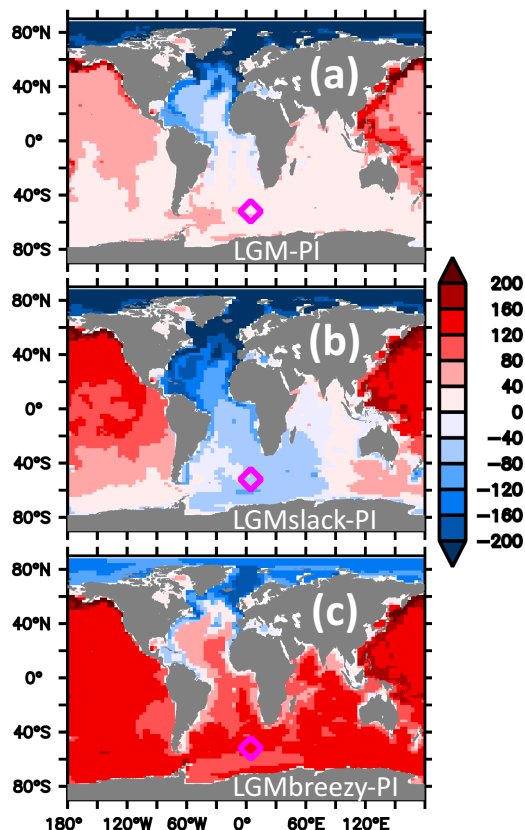


**Figure 6.** Simulated oxygen concentration at the bottom of the ocean relative to simulated preindustrial (PI) concentrations in units  $\text{mmol O}_2 \text{m}^{-3}$ . Panel (a), (b) and (c) refer to simulations *LGM*, *LGMslack* and *LGMbreezy*, respectively.

532

### 533 4.3 Model Uncertainties

534 Assessing the reliability of model projections is not straight-forward. This applies  
 535 to both, climate models (Notz, 2015) and pelagic biogeochemical models (Löptien and  
 536 Dietze, 2017). Our approach here is to highlight two of our simplifying *ad-hoc* assumptions  
 537 which may potentially degrade our model results. One of these assumptions concerns the  
 538 DSi supply by rivers. In our simulations, all DSi supplied from the land into the ocean  
 539 is homogeneously distributed over the oceans. The rationale behind this is the sparse  
 540 information available on glacial-interglacial changes in river loads and the implicit  
 541 assumption that horizontal transports act on much shorter timescales than the vertical  
 542 transports. Among the (unintended) consequences is a glacial Arctic Ocean which is  
 543 continuously flushed by isotopically light DSi in our model - even though - in reality, it was  
 544 covered by ice and probably did not receive any river runoff at all.

545 Another simplification in our setup is not to account for isotopic fractionation during  
 546 BSi dissolution - an approach we share with the pioneering 3-dimensional modeling

work of Wischmeyer et al. (2003), the box modeling work of Reynolds (2009), and the 3-dimensional modeling work of Gao et al. (2016). Our simulation of deep  $\delta^{30}\text{Si}$  of DSi (see, Figure A.6) fits into this successive model development in that it features a realistic gradient in the deep waters of the Atlantic and Pacific Oceans. In comparison, the early work of Wischmeyer et al. (2003) failed to simulate a significant gradient (less than 0.1‰ difference), while Reynolds (2009) and Gao et al. (2016) reported a more realistic difference of 0.3‰ between the basins. Our model features 0.5‰ which is even closer to the data-constrained model estimate of 0.7‰ by Holzer and Brzezinski (2015) - arguably the most comprehensive estimate of today's  $\delta^{30}\text{Si}$  of DSi distribution in the deep ocean. Further comparison with the Holzer and Brzezinski (2015) estimate, however, reveals that our simulated variance in the deep Pacific is apparently too low: while results by Holzer and Brzezinski (2015) suggest a range between 1.7‰ in the South and 1.1‰ up North, we find barely any variation in our simulation *PI*. According to Holzer and Brzezinski (2015) and Beucher et al. (2008) this deficiency of our model is linked to not accounting for isotopic fractionation during BSi dissolution.

Another problematic region where our model simulations deviate from observations of  $\delta^{30}\text{Si}$  of BSi is the eastern equatorial Pacific in Fig. 3 and 4. We speculate that this is associated with an unrealistic zonal circulation in our model which is apparently endemic to the current generation of coupled ocean circulation biogeochemical models (Dietze and Lötjien, 2013; Getzlaff and Dietze, 2013).

In summary, we refer to a model that is capable of reproducing the effects of (pre-industrial) circulation and isotopic fractionation during BSi production with a fidelity comparable to existing non data-assimilated 3-dimensional coupled ocean circulation biogeochemical models. Compared with the arguably most comprehensive data-assimilated model estimate of the present abyssal  $\delta^{30}$  of DSi we miss an intra-basin variability in the Pacific Ocean that is probably linked to unaccounted isotopic fractionation during BSi dissolution.

## 5 Conclusions

We set out to simulate  $\delta^{30}\text{Si}$  of BSi (such as opal) archived in oceanic sediments under modern climates (PI) and glacial conditions (LGM). Specifically, we implement and test several hypothesis which were suggested in the literature to explain the observed difference in  $\delta^{30}\text{Si}$  of BSi between PI and LGM.

Our numerical experiments with an Earth System Model of intermediate complexity suggest that neither of the following processes effected glacial-interglacial changes in the isotopic composition of BSi is consistent with observations: (1) an overall cooling and substantial reduction of the meridional overturning circulation (our experiment *LGM*), (2) a decrease of Si:N quota in diatoms as potentially effected by increased air-sea iron fluxes (our experiment *LGMfe*), (3) decreasing winds (our experiment *LGMslack*) and (4) increasing or decreasing Si supply to the ocean (our experiments *LGMtrickle* and *LGMflush*).

Out of seven sensitivity experiments, only the simulation with increased winds (experiment *LGMbreezy*) and the simulation with a changed isotopic composition of river runoff (experiment *LGMlight*) reproduce the observed sign of change, specifically in the SO. The experiment with increasing winds (experiment *LGMbreezy*), however, fails to reproduce the magnitude of observed changes and is, furthermore, inconsistent with the Jaccard et al. (2016) estimate of dissolved near-bottom oxygen concentrations (based on redox-sensitive trace-metal records archived in the sediments in the Atlantic Sector of the SO). The experiment *LGMlight* is most consistent with observed changes in  $\delta^{30}\text{Si}$  of BSi in terms of both, sign and magnitude. This confirms the suggestions by Frings et al. (2016) that changes in the isotopic composition of DSi supplied to the ocean (rather than

597 changes in the internal oceanic cycling of DSi) triggered low glacial  $\delta^{30}\text{Si}$  of BSi. Fur-  
 598 ther, the estimated manifestation timescale of changes in  $\delta^{30}\text{Si}$  of BSi range between sev-  
 599 eral hundreds to 2500 years at the observational sites. This means that the respective  
 600 signal should be detectable - despite a global turnover timescale of DSi, which is com-  
 601 parable to the period of glacial-interglacial cycles.

602 As a side aspect we find a simulated oceanic DSi inventory which is 10-20% lower  
 603 during the Last Glacial Maximum than today. This is somewhat counterintuitive because  
 604 simulated BSi production is also lower during the LGM which suggests that less BSi is  
 605 sinking down to the oceanic sediment. More comprehensive analysis shows that this ef-  
 606 fect is outweighed by BSi dissolution rates that are also slowed down as a consequence  
 607 of colder temperatures such that more BSi escapes dissolution prior to sedimentation in  
 608 our model.

609 Caveats remain. A major problem of developing a Si module within the framework  
 610 of an Earth System Model is the high computational cost associated with running test  
 611 simulations to equilibrium. To this end, a turnover timescale of Si in the ocean of more  
 612 than 10 000 years is a real handicap. Among the simplifications we chose in order to limit  
 613 the number of test simulations was discarding the effect of fractionation during BSi dis-  
 614 solution. According to Holzer and Brzezinski (2015) and Beucher et al. (2008) this may  
 615 be the reason why our model does not reproduce observed variations of  $\delta^{30}\text{Si}$  of DSi within  
 616 the Pacific. Further - substantial - uncertainty is added by the generic problem of con-  
 617 straining global biogeochemical ocean models (Löptien and Dietze (2015); Löptien and  
 618 Dietze (2017); Löptien and Dietze (2019)).

## 619 A Model Assessment

620 The UVic ESCM reference version we use for *LGM* and *PI* has been described and  
 621 assessed by Brennan et al. (2012). We left this base module unchanged. In the follow-  
 622 ing we refer to our extension adding an Si-cycle (which does not feedback onto the orig-  
 623 inal modules) in the following.

624 Figure A.1 shows the modern climate (PI) simulated DSi concentrations at the sur-  
 625 face and at depth compared to observations (Garcia et al., 2010). A comparison of panel  
 626 (a) and (c) suggests that the simulated DSi concentrations are somewhat too high at the  
 627 surface, specifically in the tropics and the southern part of the Southern Ocean. At the  
 628 same time, DSi concentrations are too low at the bottom, specifically in the northern Pa-  
 629 cific (panel (b) and (d)). These deviations are also visible in the global mean profiles in  
 630 Fig. A.2.

**Table A.1.** Comparison between observations (OBS) and preindustrial simulation (*PI*). Temp., Sal., std., RMS, corr. coeff., var refer to temperature, salinity, standard deviation, root mean square error between PI and OBS, and variance, respectively.  $\delta^{30}\text{DSi}$  refers to surface values. The origin of observations is documented in Section 2.1.

variable	unit	std. OBS	std. <i>PI</i>	bias ( <i>PI</i> -OBS)	RMS	corr. coeff.	var( <i>PI</i> ref)/ var(OBS)
Temp.	$^{\circ}\text{C}$	6.5	6.6	0.6	1.4	0.98	103%
Sal.	<i>PSU</i>	0.6	0.5	0.03	0.3	0.85	70%
$\text{PO}_4$	$\text{mmol P m}^{-3}$	0.83	0.77	-0.03	0.3	0.94	86%
DSi	$\text{mmol Si m}^{-3}$	54	40	11	30	0.84	54%
$\delta^{30}\text{DSi}$	$\text{‰}$	0.62	0.48	0.57	0.56	0.51	60%

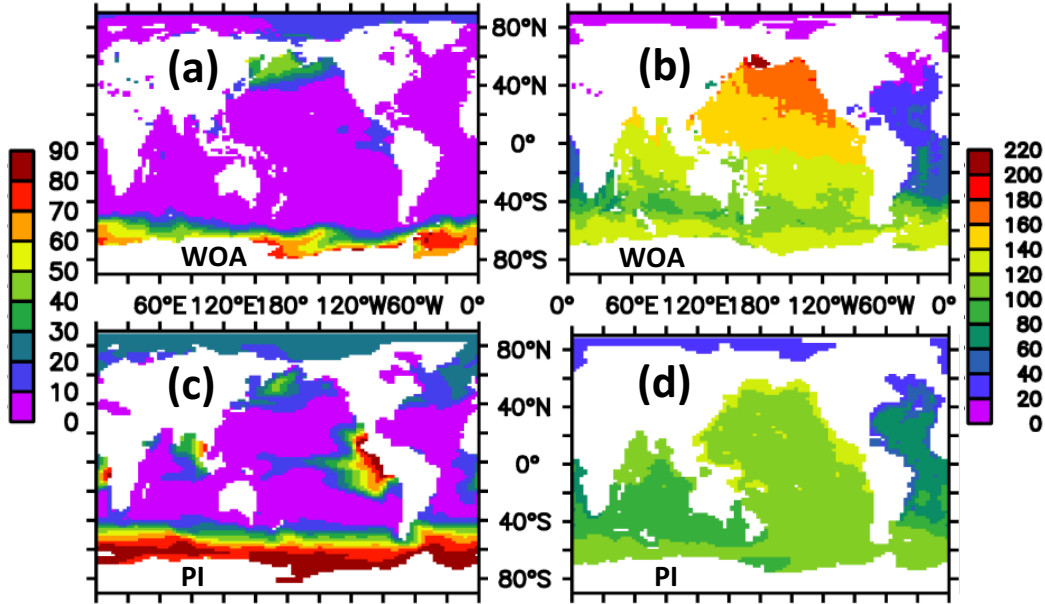


**Figure A.1.** Surface and deep (2000 m to bottom average) DSi concentrations in units  $\text{mmol Si/m}^3$ . (a) and (b) refer to surface and abyssal observations (Garcia et al., 2010), respectively. (c) and (d) refer to simulated preindustrial (PI) surface and abyssal concentrations, respectively.

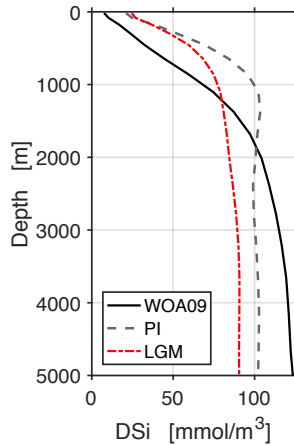


**Figure A.2.** Zonally and meridionally averaged vertical profile of DSi concentrations in units  $\text{mmol Si/m}^3$ . The black, grey dashed, and red dot-dashed lines refer to observations (black line, Garcia et al., 2010), preindustrial simulation, and Last Glacial Maximum simulation, respectively.

631 We suspect that these differences are both the result of our choice of parameters  
 632 (possibly an underestimated opal sinking velocity and an underestimated molecular DSi  
 633 to phosphate stoichiometric ratio or an underestimated BSi production rate) as well as  
 634 being caused by rather coarse spatial resolution of the ocean module which is known to  
 635 retard ocean transports (e.g. Getzlaff and Dietze, 2013). Figure A.3 depicts the zonally  
 636 averaged export of DSi. While the above mentioned biases map also onto this metric,  
 637 the major features are, nevertheless, captured. Specifically the trapping of DSi in the

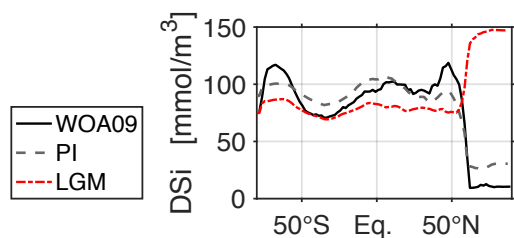


**Figure A.3.** Zonally and vertically averaged DSi concentrations in units  $mmol Si m^{-3}$ . The black, grey dashed, and red dot-dashed lines refer to observations (black line, Garcia et al., 2010), preindustrial simulation, and Last Glacial Maximum simulation, respectively.

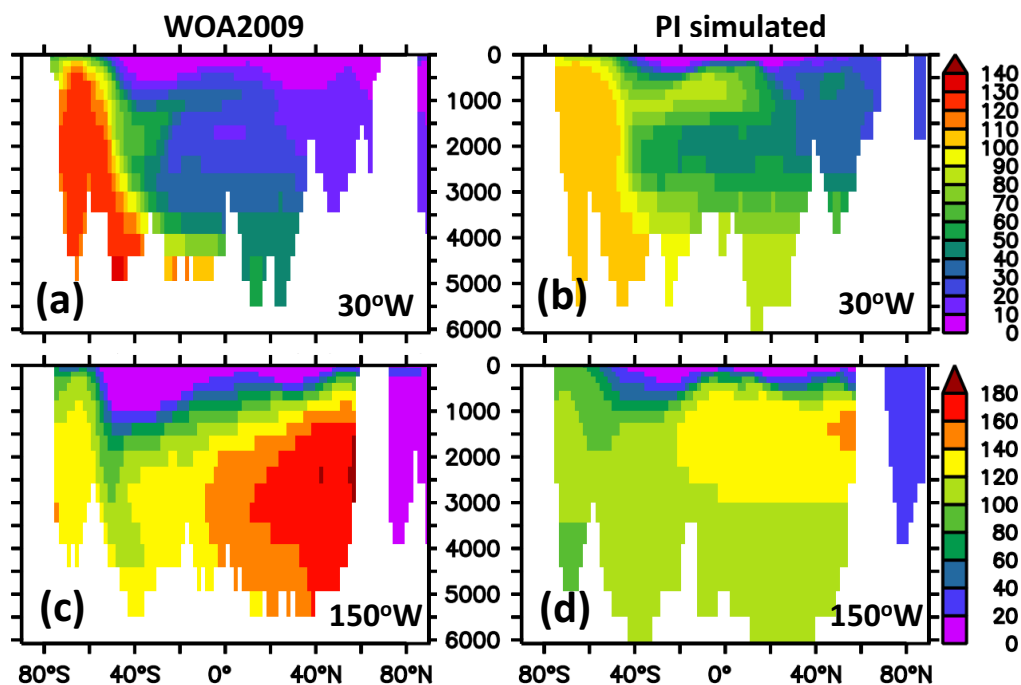


**Figure A.4.** Meridional sections over depth (in m) of DSi in units  $mmol Si m^{-3}$ . Panel (a) and (c) refer to observations (Garcia et al., 2010) and panel (b) and (d) to the preindustrial simulation.

638 SO, high values in the tropics and a large drop in the Arctic are clearly visible. Not well  
 639 captured are, however, the mid latitudes in the northern hemisphere where the simulated  
 640 export is underestimated. Further, the transition zone to the SO is not as sharp as observed  
 641 and DSi values in the Arctic are somewhat overestimated.

642 The Figures A.4 and A.5 show meridional sections of both, simulated DSi and  
 643 phosphate in comparison to the observations. This allows for a continuative exploration  
 644 of the reasons for model-data mismatches with respect to DSi : the section through the  
 645 Atlantic (at 30°W) shows simulated DSi concentrations that are generally underestimated  
 646 while phosphate seems in better agreement with the observations in that respect. In the  
 647 SO, however, both variables are biased - and the biases oppose one another: in terms  
 648 of SO nutrient trapping, simulated phosphate is trapped more efficiently than indicated  
 649 by the observations. This is in contrast to simulated DSi concentrations, where the sim-  
 650 ulated SO nutrient trapping is too weak. With one nutrient biased high and the other

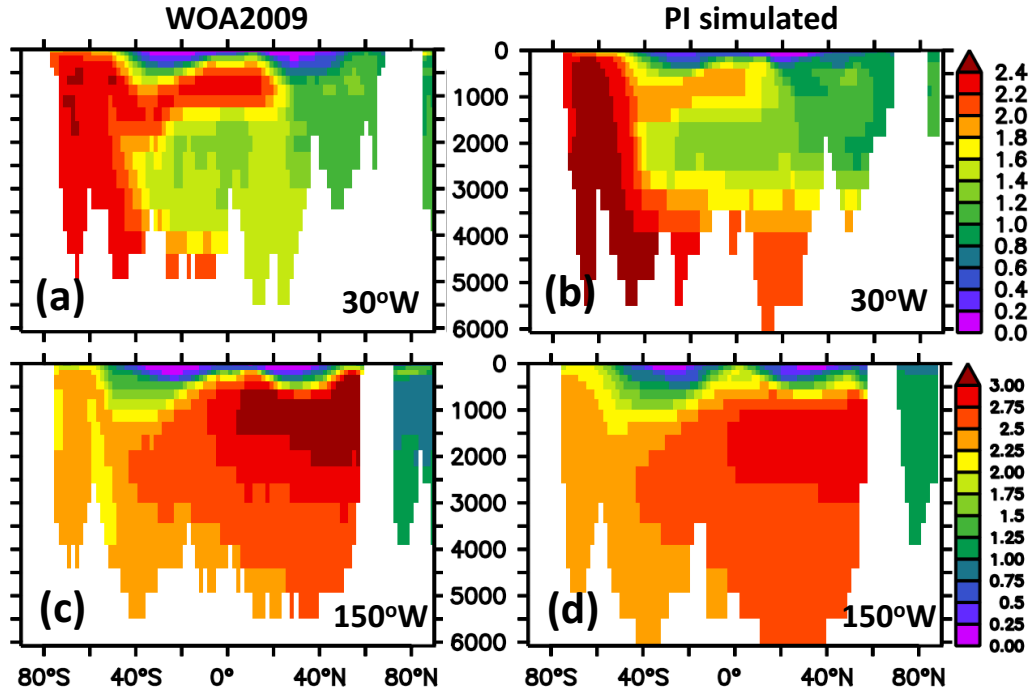


**Figure A.5.** Meridional sections over depth (in m) of PO<sub>4</sub> in units  $\text{mmol Si m}^{-3}$ . Panel (a) and (c) refer to observations (Garcia et al., 2010) and panel (b) and (d) to the preindustrial simulation.

651 nutrient biased low it seems unlikely that a deficient circulation is the cause for these  
 652 biases (although this can not be ruled out). This suggests that the SO nutrient trapping  
 653 relates strongly to the biogeochemical model parameters. One conclusion from this may  
 654 be that the biogeochemical model is better tuned with respect to phosphate than to DSi.  
 655 This is to be expected because of the wider use of the phosphate-based biogeochemical  
 656 model and the much shorter equilibration time scales for phosphate which facilitate the  
 657 respective tuning to observations. In the Pacific, however, the situation differs, and sub-  
 658 surface maxima in the northern hemisphere (except the Arctic) are too low for both phos-  
 659 phosphate and DSi. Following our reasoning above this may be indicative for flaws in the ocean  
 660 circulation module. Please note, however, that the attribution of flaws in model behav-  
 661 ior to respective processes is challenging and may even be impossible given the current  
 662 set of observations (e.g. Löptien and Dietze, 2019).

663 Table A.1 provides a quantitative estimate of how our DSi/BSi module compares  
 664 against the underlying biogeochemical and ocean circulation module of Brennan et al.  
 665 (2012). The simulated temperature variance is overestimated by 3% and the tempera-  
 666 ture bias is 0.6 K, corresponding to 9% relative to the standard deviation in the obser-  
 667 vations. The respective bias to standard deviation of salinity is with 0.03 even smaller  
 668 (5% relative to the standard deviation in the observations). Simulated phosphate con-  
 669 centrations are, surprisingly, even closer to observations than simulated salinities: the  
 670 bias to standard deviation ratio is smaller (4%) and the simulated variance covers 86%  
 671 of observed levels (versus 70% for salinity). Given that the salinity distribution directly  
 672 affects ocean circulation via density driven pressure gradients, it is remarkable that the  
 673 misfit in this active physical property can be much larger than the misfit of the rather  
 674 passive (in terms of their effect on circulation) phosphate whose distribution is directly  
 675 shaped by oceanic circulation. This may be an indication that the biogeochemical mod-

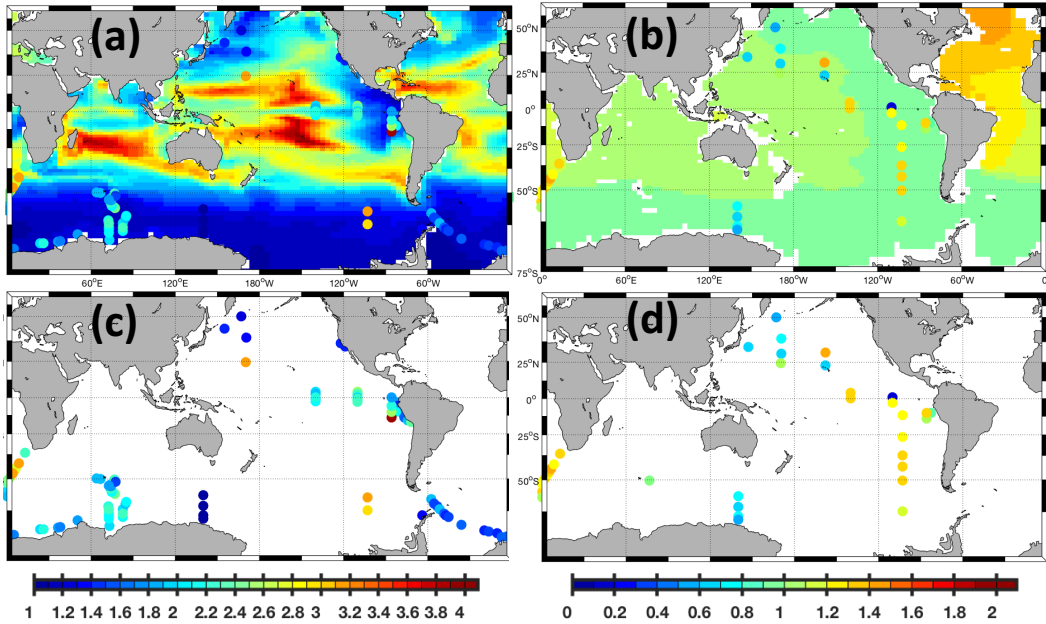


**Figure A.6.**  $\delta^{30}DSi$  at the surface (50 m, panel (a) & (c)) and at depth (2000 m, panel (b) & (d)) in units ‰. The colored blobs denote those observations (see Section 2.1) within 0-100 m (1500-2500 m) that are closest to the nominal depth of 50 m (2000 m). The background color in panel (a) and (b) refers to simulation PI. Panel (c) and (d) show respective observations only to facilitate their recognition.

676     ule of Brennan et al. (2012) has been "overly successfully" tuned to a flawed physics (a  
 677     process illustrated by Löptien and Dietze, 2019). In contrast, the simulated DSi features  
 678     the largest deviations among the metrics reviewed here. The simulation features a vari-  
 679     ance corresponding to 54% of observed levels and the simulated bias is 21% relative to  
 680     the observed standard deviation. The correlation of simulated DSi concentrations with  
 681     observations is, however, rather good in the sense that it is very similar to that of salin-  
 682     ity (0.84 versus 0.85).

683     Fig. A.6 shows our simulated preindustrial  $\delta^{30}DSi$  distribution. The sparseness of  
 684     observational data with often times puzzling inhomogeneities illustrates the Hendry and  
 685     Brzezinski (2014) conclusion that the  $\delta^{30}DSi$  data set is "... inadequate to evaluate mech-  
 686     anisms leading to even the first-order distribution of isotopes of Si in the global ocean".  
 687     Also we are urged to compare point observations to large scale averages, resolved by the  
 688     model. The relatively low correlation of 0.51 between model and observations has thus  
 689     to be considered with some caution.

690 **Acknowledgments**

691 H. D. and U. L. acknowledge funding by Deutsche Forschungsgemeinschaft (DFG) in the  
692 framework of the priority program *Antarctic Research with comparative investigations*  
693 *in Arctic ice areas SPP 1158* by grant no. *SCHN 762/5-1*. We acknowledge discussions  
694 with Mark Holzer and Katrin Meissner. Katrin Meissner provided the model configura-  
695 tion by sharing code and forcing files. Fruitful discussion with Richard Matear and An-  
696 drew Lenton were made possible by DFG grant no. *DI 1665/6-1* and *LO 1377/5-1*. A  
697 number of very good review papers eased the entry of H. D. and U. L. into the field. We  
698 are grateful to each and everyone sharing observational data. Data is available through  
699 Locarnini et al. 2010, Antonov et al. 2010, Garcia et al. 2010, Beucher et al. 2008, Car-  
700 dinal et al. 2005, De La Rocha et al. 2011, de Souza et al. 2012, Ehlert et al. 2012, Fripi-  
701 at et al. 2011, Grasse et al. 2013, Reynolds et al. 2006, Frings et al. 2016, Brzezinski  
702 et al. 2002, De La Rocha et al. 1997, De La Rocha et al. 1998, De La Rocha et al. 2011,  
703 Ehlert et al. 2013, Ellwood et al. 2010, Hendry et al. 2012, Horn et al. 2011, and Pichevin  
704 et al. 2009.

## References

- 705
- 706 Antonov, J. I., Seidov, D., Boyer, T. P., Locarnini, R. A., Mishonov, A. V., Garcia,  
707 H. E., Baranova, O. K., Zweng, M. M., and Johnson, D. R., (2010). World  
708 Ocean Atlas 2009, Volume 2: Salinity. S. Levitus, Ed. NOAA Atlas NESDIS  
709 69, U.S. Government Printing Office, Washington, D.C., 184pp.
- 710 Basile-Doelsch, I., (2006). Si stable isotopes in the Earth's surface: A review. *Journal*  
711 *of Geochemical Exploration*, 88, 252–256, doi:10.1016/j.gexplo.2005.08.050.
- 712 Bauer, P., Thorpe, A., and Brunet, G., (2015). The quiet revolution of numerical  
713 weather prediction. *Nature*, 525, 7567, 47–55, doi:10.1038/nature14956.
- 714 Beucher, C. P., Brzezinski, M. A., and Jones, J. L., (2008). Sources and biological  
715 fractionation of Silicon isotopes in the Eastern Equatorial Pacific. *Geochimica*  
716 *et Cosmochimica Acta*, 72, 3063–3073, doi:10.1016/j.gca.2008.04.021.
- 717 Beucher, C. P., Brzezinski, M. A., and Jones, J. L., (2011). Mechanisms controlling  
718 silicon isotope distribution in the Eastern Equatorial Pacific. *Geochimica et*  
719 *Cosmochimica Acta*, 75, 4286–4294, doi:10.1016/j.gca.2011.05.024.
- 720 Braconnot, P., Harrison, S. P., Kageyama, M., Bartlein, P. J., Masson-Delmotte,  
721 V., Abe-Ouchi, A., Otto-Bliesner, B., and Zhao, Y., (2012). Evaluation of cli-  
722 mate models using palaeoclimatic data. *Nature Climate Change*, 2, 417–424,  
723 doi:10.1038/NCLIMATE1456.
- 724 Brennan, C. E., Weaver, A. J., Eby, M., and Meissner, K. J., (2012). Modelling Oxy-  
725 gen Isotopes in the University of Victoria Earth System Climate Model for  
726 Preindustrial and Last Glacial Maximum Conditions. *Atmosphere-Ocean*, 50,  
727 4, 447–465, doi:10.1080/07055900.2012.707611.
- 728 Brzezinski, M. A., Pride, C. J., Franck, V. M., Sigman, D. M., Sarmiento, J. L.,  
729 Matsumoto, K., Gruber, N., Rau, G. H., and Coale, K. H., (2002). A switch  
730 from  $\text{Si}(\text{OH})_4$  to  $\text{NO}_3^-$  depletion in the glacial Southern Ocean. *Geophysical*  
731 *Research Letters*, 29, 12, 1564, doi:10.1029/2001GL014349.
- 732 Cardinal, D., Alleman, L. Y., Dehairs, F., Savoye, N., Trull, T. W., and André, L.,  
733 (2005). Relevance of silicon isotopes to Si-nutrient utilization and Si-source  
734 assessment in Antarctic waters. *Global Biogeochemical Cycles*, 19, GB2007,  
735 doi:10.1029/2004GB002364.
- 736 Closset, I., Cardinal, D., Rembauville, M., Thil, F., and Blain, S., (2016). Un-  
737 veiling the Si cycle using isotopes in an iron-fertilized zone of the Southern  
738 Ocean: from mixed-layer supply to export. *Biogeosciences*, 13, 6049–6066,  
739 doi:10.5194/bg-13-6049-2016.
- 740 Coplen, T. B., Hopple, J. A., Böhlke, J. K., Peiser, H. S., Rieder, S. E., Krouse,  
741 H. R., Rosman, K. J. R., Ding, T., Vocke, Jr., R. D., Révész, K. M., Lamberty,  
742 A., Taylor, P., and De Bièvre, (2002). *Compilation of Minimum and Maximum*  
743 *Isotope Ratios of Selected Elements in Naturally Occurring Terrestrial Materi-*  
744 *als and Reagents*, Water-Resources Investigation Report, 01-4222, 1–110, U.S.  
745 Department of the Interior and U.S. Geological Survey, Reston Virginia.
- 746 De La Rocha, C. L., Brzezinski, M. A., and De Niro, M. J., (1998). Fractiona-  
747 tion of silicon isotopes by marine diatoms during biogenic silica formation.  
748 *Geochimica et Cosmochimica Acta*, 61, 23, 5051–5056, doi:10.1016/S0016-  
749 7037(97)00300-1.
- 750 De La Rocha, C. L., Brzezinski, M. A., De Niro, M. J., and Shemesh, A., (1998).  
751 Silicon-isotope composition of diatoms as an indicator of past oceanic change.  
752 *Nature*, 395, 680–683, doi:10.1038/27174.
- 753 De La Rocha, C. L., Bescont, P., Croguennoc, A., Ponzevera, E., (2011). The sili-  
754 con isotopic composition of surface waters in the Atlantic and Indian sectors  
755 of the Southern Ocean. *Geochimica et Cosmochimica Acta*, 75, 5283–5295,  
756 doi:10.1016/j.gca.2011.06.028.
- 757 de Souza, G. F., Reynolds, B. C., Johnson, G. C., Bullister, J. L., and Bourdon, B.,  
758 (2012a). Silicon stable isotope distribution traces Southern Ocean export of Si  
759 to the South Pacific thermocline. *Biogeosciences*, 9, 4199–4213, doi:10.5194/bg-

- 9-4199-2012.
- 760 de Souza, G. F., Reynolds, B. C., Rickli, J., Frank, M., Saito, M. A., Gerringa,  
761 L. J. A., and Bourdon, B., (2012). Southern Ocean control of silicon stable  
762 isotope distribution in the deep Atlantic Ocean. *Global Biogeochemical Cycles*,  
763 26, GB2035, doi:10.1029/2011GB004141.
- 764 Dietze, H., and Löptien, U., (2013). Revisiting "nutrient trapping" in global coupled  
765 biogeochemical ocean circulation models. *Global Biogeochemical Cycles*, 27,  
766 265–284, doi:10.1002/gbc.20029.
- 767 Ehlert C., Grasse, P., Mollier-Vogel, E., Bösch, T., Franz, J., de Souza, G. F.,  
768 Reynolds, B. C., Stramma, L., and Frank, M., (2012). Factors controlling  
769 the silicon isotope distribution in waters and surface sediments of the Pe-  
770 ruvian coastal upwelling. *Geochimica et Cosmochimica Acta* 99, 128–145,  
771 doi:10.1016/j.gca.2012.09.038.
- 772 Ehlert, C., Grasse, P., and Frank, M., (2013). Changes in silicate utilisation and  
773 upwelling intensity off Peru since the Last Glacial Maximum - insights from  
774 silicon and neodymium isotopes. *Quaternary Science Reviews*, 72, 18–35,  
775 doi:10.1016/j.quascirev.2013.04.013.
- 776 Ellwood, M. J., Wille, M., and Maher, W., (2010). Glacial Silicic Acid Con-  
777 centration in the Southern Ocean. *Science*, 330, 6007, 1088–1091,  
778 doi:10.1126/science.1194614.
- 779 Franck, V. M., Brzezinski, M. A., Coale, K. H., and Nelson, D. M., (2000). Iron  
780 and silicic acid concentrations regulate Si uptake north and south of the Polar  
781 Frontal Zone in the Pacific Sector of the Southern Ocean. *Deep-Sea Research*  
782 *Part II*, 47, 3315–3338, doi:10.1016/S0967-0645(00)00070-9.
- 783 Frings, P. J., Clymans, W., Fontorbe, G., De La Roche, C. L., and Conley, D. J.,  
784 (2016). The continental Si cycle and its impact on the ocean Si isotope budget.  
785 *Chemical Geology*, 425, 12–36, doi:10.1016/j.chemgeo.2016.01.020.
- 786 Fripiat, F., Cavagna, A.-J., Dehairs, F., Speich, S., André, L., and Cardinal, D.,  
787 (2011). Silicon pool dynamics and biogenic silica export in the Southern Ocean  
788 inferred from Si-isotopes. *Ocean Science*, 7, 533–547, doi:10.5194/os-7-533-  
789 2011.
- 790 Fripiat, F., Cavagnam A.-J., Savoye, N., Dehairs, F., André, L., and Cardinal, D.,  
791 (2011). Isotopic constraints on the Si-biogeochemical cycle of the Antarc-  
792 tic Zone in the Kerguelen area (KEOPS). *Marine Chemistry*, 123, 11–22,  
793 doi:10.1016/j.marchem.2010.08.005.
- 794 Fripiat, F., Cavagna, A.-J., Dehairs, F., de Brauwere, A., André, L., and Cardinal,  
795 D., (2012). Processes controlling the Si-isotopic composition in the Southern  
796 Ocean and application for paleoceanography. *Biogeosciences*, 9, 2443–2457,  
797 doi:10.5194/bg-9-2443-2012.
- 798 Gao, S., Wolf-Gladrow, D. A., and Völker, C., (2016). Simulating the modern  $\delta^{30}\text{Si}$   
799 distribution in the oceans and in marine sediments. *Global Biogeochemical*  
800 *Cycles*, 30, 120–133, doi:10.1002/2015GB005189.
- 801 Garcia, H. E., Locarnini, R. A., Boyer, T. P., and Antonov, J. I., (2010). *World*  
802 *Ocean Atlas 2009, Volume 4: Nutrients (phosphate, nitrate, silicate)*. S. Levi-  
803 tus, Ed. NOAA Atlas NESDIS 71, U.S. Government Printing Office, Washing-  
804 ton, D.C., 398 pp.
- 805 Grasse, P., Ehlert, C., and Frank, M., (2013). The influence of water mass mixing on  
806 the dissolved Si isotope composition in the Eastern Equatorial Pacific. *Earth*  
807 *and Planetary Science Letters*, 380, 60–71, doi:10.1016/j.epsl.2013.07.033.
- 808 Getzlaff, J., and Dietze, H., (2013). Effects of increased isopycnal diffusivity mimick-  
809 ing the unresolved equatorial intermediate current system in an earth system  
810 climate model. *Geophysical Research Letters*, 40, 10, doi:10.1002/grl.50419.
- 811 Hendry, K. R., and Brzezinski, M. A., (2014). Using silicon isotopes to un-  
812 derstand the role of the Southern Ocean in modern and ancient bio-  
813 geochemistry and climate. *Quaternary Science Reviews*, 89, 13–26,  
814

- 815 doi:10.1016/j.quascirev.2014.01.019.
- 816 Hendry, K. R., Robinson, L. F., Meredith, M. P., Mulitza, S., Chiessi, C. M.,  
817 and Arz, H., (2012). Abrupt changes in high-latitude nutrient supply  
818 to the Atlantic during the last glacial cycle. *Geology*, 40, 2, 123–126,  
819 doi:10.1130/G32779.1.
- 820 Holzer, M., and Brzezinski, M. A., (2016). Controls on the silicon isotope distri-  
821 bution in the ocean: New diagnostics from a data-constrained model. *Global*  
822 *Biogeochemical Cycles*, 29, 267–287, doi:10.1002/2014GB004967.
- 823 Horn, M., Beucher, C. P., Robinson, R. S., and Brzezinski, M. A., (2011). Southern  
824 ocean nitrogen and silicon dynamics during the last deglaciation. *Earth and*  
825 *Planetary Science Letters* 310, 334–339, doi:10.1016/j.epsl.2011.08.016.
- 826 Hülse, D., Arndt, S., Wilson, J. D., Munhoven, G., and Ridgwell, A., (2017).  
827 Understanding the causes and consequences of past marine carbon cy-  
828 cling variability through models. *Earth-Science Reviews* 171, 349–382,  
829 doi:10.1016/j.earscirev.2017.06.004.
- 830 Hutchins, D. A., and Bruland, K. W., (1998). Iron-limited diatom growth and  
831 Si:N uptake ratios in a coastal upwelling regime. *Nature*, 393, 561–564,  
832 doi:10.1038/31203.
- 833 Jaccard, S. L., and Galbraith, E. D., (2011). Large climate-driven changes of oceanic  
834 oxygen concentrations during the last deglaciation. *Nature Geoscience*, 5, 151–  
835 156, doi:10.1038/NGEO1352.
- 836 Jaccard, S. L., Galbraith, E. D., Martínez-García, A., and Anderson, R. F., (2016).  
837 Covariation of deep Southern Ocean oxygenations and atmospheric CO<sub>2</sub>  
838 through the last ice age. *Nature*, 530, doi:10.1038/nature16514.
- 839 Kamatani, A., (1992). Dissolution Rates of Silica from Diatoms Decomposition at  
840 Various Temperatures. *Marine Biology*, 68, 91–96.
- 841 Knutti, R., Furrer, R., Tebaldi, C., Cermak, J., and Meehl, G. A., (2009). Challenges  
842 in Combining Projections from Multiple Climate Models. *Journal of Climate*,  
843 2739–2758, doi:10.1175/2009JCLI3361.1.
- 844 Kohlfeld, K. E., Graham, R. M., de Boer, A. M., Sime, L. C., Wolff, E. W., Le  
845 Quéré, C., and Bopp, L., (2013). Southern Hemisphere westerly wind changes  
846 during the Last Glacial Maximum: paleo-data synthesis. *Quaternary Science*  
847 *Reviews*, 68, 76–95, doi:10.1016/j.quascirev.2013.01.017.
- 848 Kriest, I., and Oschlies, A., (2008). On the treatment of particulate organic matter  
849 sinking in large-scale models of marine biogeochemical cycles. *Biogeosciences*,  
850 5, 55–72, doi:10.5194/bg-5-55-2008.
- 851 Lagarias, J. C., Reeds, J. A., Wright, M. H., and Wright, P. E., (1998). Covergence  
852 Properties of the Nelder–Mead Simplex Method in Low Dimensions. *SIAM*  
853 *Journal on Optimization*, 9, 1, 112–147, doi:10.1137/S1052623496303470.
- 854 Locarnini, R. A., Mishonov, A. V., Antonov, J. I., Boyer, T. P., Garcia, H. E., Bara-  
855 nova, O. K., Zweng, M. M., and Johnson, D. R., (2010). *World Ocean Atlas*  
856 2009, Volume 1: Temperature. S. Levitus, Ed. NOAA Atlas NESDIS 68, U.S.  
857 Government Printing Office, Washington, D.C., 184 pp.
- 858 Löptien, U., and Dietze, H., (2015). Constraining parameters in marine pelagic  
859 ecosystem models - is it actually feasible with typical observations of standing  
860 stocks? *Ocean Science*, 11, 4, 573–590, doi:10.5194/os-11-573-2015.
- 861 Löptien, U., and Dietze, H., (2017). Effects of parameter indeterminacy in pelagic  
862 biogeochemical modules of Earth System Models on projections into a warm-  
863 ing future: The scale of the problem. *Global Biogeochemical Cycles*, 31, 7,  
864 1155–1172, doi:10.1002/2017GB005690.
- 865 Löptien, U., and Dietze, H., (2019). Reciprocal bias compensation and ensuing un-  
866 certainties in model-based climate projections: pelagic biogeochemistry versus  
867 ocean mixing. *Biogeosciences*, 16, 1865–1881, doi:10.5194/bg-16-1865-2019.
- 868 Margo Project Members, (2009). Constraints on the magnitude and patterns of  
869 ocean cooling at the Last Glacial Maximum. *Nature Geoscience*, 2, 127–132,

- 870 doi:10.1038/NGEO411.
- 871 Matsumoto, K., Chase, Z., and Kohfeld, K., (2014). Different mechanisms of silicic  
872 acid leakage and their biogeochemical consequences. *Paleoceanography*, 29,  
873 doi:10.1002/2013PA002588.
- 874 Matsumoto, K., Sarmienta, J. L., and Brzezinski, M. A., (2002). Silicic acid leak-  
875 age from the Southern Ocean: A possible explanation for glacial atmospheric  
876  $p\text{CO}_2$ . *Global Biogeochemical Cycles*, 16, 3, 1031, doi:10.1029/2001GB001442.
- 877 McGee, D., Broecker, W. S., and Winckler, G., (2010). Gustiness: The driver  
878 of glacial dustiness? *Quaternary Science Reviews*, 29, 17-18, 2340–2350,  
879 doi:10.1016/j.quascirev.2010.06.009.
- 880 Moore, J. K., Fu, W., Primeau, F., Britten, G. L., Lindsay, K., Long, M., Doney,  
881 S., Mahowald, N., Hoffman, F., and Randerson, J., (2018). Sustained climate  
882 warming drives declining marine biological productivity. *Science*, 359, 6380,  
883 1139–1143, doi:10.1126/science.aao6379.
- 884 Notz, D., (2015). How well must climate models agree with observations?  
885 *Philosophical Transactions of the Royal Society A.*, 373, 20140164,  
886 doi:10.1098/rsta.2014.0164.
- 887 Peltier, W. R. (1994). Ice age paleotopography. *Science*, 265(5169), 195-201,  
888 doi:10.1126/science.265.5169.195.
- 889 Pichevin, L. E., Reynolds, B. C., Ganeshram, R. S., Cacho, I., Pena, L., Keefe,  
890 K., and Ellam, R. M., (2009). Enhanced carbon pump inferred from relax-  
891 ation of nutrient limitation in the glacial ocean. *Nature*, 459, 1114–1117,  
892 doi:10.1038/nature08101.
- 893 Pondaven, P., Ruiz-Pino, D., Fravallo, C., Tréguer, P., and Jeandel, C., (2000). In-  
894 terannual variability of *Si* and *N* cycles at the time-series station KERFIX  
895 between 1990 and 1995 - a 1-D modelling study. *Deep Sea Research I*, 47,  
896 223–257, doi:10.1016/S0967-0637(99)00053-9.
- 897 Ragueneau, O., Tréguer, P., Leynaert, A., Anderson, R. F., Brzezinski, M. A., De-  
898 Master, D. J., Dugdale, R. C., Dymond, J., Fischer, G., François, R., Heinze,  
899 C., Maier-Reimer, E., Martin-Jézéquel, V., Nelson, D. M., and Quéguiner,  
900 B., (2000). A review of the Si cycle in the modern ocean: recent progress  
901 and missing gaps in the application of biogenic opal as a paleoproductiv-  
902 ity proxy. *Global and Planetary Change*, 26, 4, 317–365, doi:10.1016/S0921-  
903 8181(00)00052-7.
- 904 Rahman, S., Aller, R. C., and Cochran, J. K., (2017). The Missing Silica Sink:  
905 Revisiting the Marine Sedimentary Si Cycle Using Cosmogenic  $^{32}\text{Si}$ . *Global*  
906 *Biogeochemical Cycles*, 31, 1559–1578, doi:10.1002/2017GB005746.
- 907 Reynolds, B. C., (2009). Modeling the modern marine  $\delta^{30}\text{Si}$  distribution. *Global*  
908 *Biogeochemical Cycles*, 23, GB2015, doi:10.1029/2008GB003266.
- 909 Reynolds, B. C., Frank, M., and Halliday, A. N., (2006). Silicon isotope fractionation  
910 during nutrient utilization in the North Pacific. *Earth and Planetary Science*  
911 *Letters*, 244, 431–443, doi:10.1016/j.epsl.2006.02.002.
- 912 Richter, F. M., and Turekian, K. K., (1993). Simple models for the geochemical  
913 response of the ocean to climatic and tectonic forcing. *Earth and Planetary*  
914 *Science Letters*, 119, 1-2, 121–131, doi:10.1016/0012-821X(93)90010-7.
- 915 Rosenthal, Y., Boyle, E. A., and Labeyrie, L., (1997). Last glacial maximum  
916 paleochemistry and deepwater circulation in the Southern Ocean: Ev-  
917 idence from foraminiferal cadmium. *Paleoceanography*, 12, 6, 787–796,  
918 doi:10.1029/97PA02508.
- 919 Schoelynck, J., Subalusky, A. L., Struyf, E., Dutton, C. L., Unzué-Belmonte, D.,  
920 Van de Vijver, B., Post, D. M., Rosi, E. J., Meire, P., and Frings, P., (2019).  
921 Hippos (*Hippopotamus amphibius*): The animal silicon pump. *Science Ad-*  
922 *vances*, 5, 5 1–10, doi:10.1126/sciadv.aav0395 .
- 923 Sime, L. C., Kohfeld, K. E., Le Quééré, Wolff, E. W., de Boer, A. M., Graham,  
924 R. M., and Bopp, L., (2013). Southern Hemisphere westerly wind changes

- 925 during the Last Glacial Maximum: model-data comparison. *Quaternary Sci-*  
926 *ence Reviews*, 64, 104–120, doi:10.1016/j.quascirev.2012.12.008.
- 927 Stoll, H., (2020). 30 years of the iron hypothesis of ice ages. *Nature*, 578, 370–371,  
928 doi:10.1038/d41586-020-00393-x.
- 929 Tréguer, P., Nelson, D. N., Van Bennekom, A. J., DeMaster, D. J., Leynaert, A.,  
930 and Quéguiner, B., (1995). The Silica Balance in the World Ocean: A Reesti-  
931 mate. *Science*, 268, 5209, 375–379, doi:10.1126/science.268.5209.375 .
- 932 Weaver, A. J., Eby, M., Wiebe, E. C., Bitz, C. M., Duffy, P. B., Ewen, T. L., Fan-  
933 ning, A. F., Holland, M. M., Macfadyen, A., Matthews, H. D., Meissner, K. J.,  
934 Saenko, O., Schmittner, A., Wang, H., and Yoshimori, M., (2001). The UVic  
935 Earth System Climate Model: Model description, climatology, and applica-  
936 tions to past, present and future climates. *Atmosphere-Ocean*, 39, 361–428,  
937 doi:10.1080/07055900.2001.9649686.
- 938 Wischmeyer, A. G., De La Rocha, C., Maier-Reimer, E., and Wolf-Gladrow, D. A.,  
939 (2003). Control mechanisms for the oceanic distribution of silicon isotopes.  
940 *Global Biogeochemical Cycles*, 17, 3, 1083, doi:10.1029/2002GB002022.